


Phospholipase D2 restores endothelial barrier function by promoting PTPN14-mediated VE-cadherin dephosphorylation

Received for publication, November 11, 2019, and in revised form, April 3, 2020. Published, Papers in Press, April 23, 2020, DOI 10.1074/jbc.RA119.011801

Panfeng Fu^{1,2}, Ramaswamy Ramchandran¹, Mark Shaaya¹, Longshuang Huang¹, David L. Ebenezer¹, Ying Jiang³, Yulia Komarova¹, Stephen M. Vogel¹, Asrar B. Malik¹, Richard D. Minshall^{1,3}, Guangwei Du⁴ , Nicholas K. Tonks⁵, and Viswanathan Natarajan^{1,6,*}

From the Departments of ¹Pharmacology, ³Anesthesiology, and ⁶Medicine, University of Illinois, Chicago, Illinois, ²The Affiliated Hospital of Medical School, Ningbo University, Ningbo, China, ⁴Department of Integrative Biology and Pharmacology, University of Texas Health Science Center at Houston, Houston, Texas, and ⁵Cold Spring Harbor Laboratory, Cold Spring Harbor, New York

Edited by Dennis R. Voelker

Increased permeability of vascular lung tissues is a hallmark of acute lung injury and is often caused by edemagenic insults resulting in inflammation. Vascular endothelial (VE)-cadherin undergoes internalization in response to inflammatory stimuli and is recycled at cell adhesion junctions during endothelial barrier re-establishment. Here, we hypothesized that phospholipase D (PLD)-generated phosphatidic acid (PA) signaling regulates VE-cadherin recycling and promotes endothelial barrier recovery by dephosphorylating VE-cadherin. Genetic deletion of *PLD2* impaired recovery from protease-activated receptor-1-activating peptide (PAR-1-AP)-induced lung vascular permeability and potentiated inflammation *in vivo*. In human lung microvascular endothelial cells (HLMVECs), inhibition or deletion of *PLD2*, but not of *PLD1*, delayed endothelial barrier recovery after thrombin stimulation. Thrombin stimulation of HLMVECs increased co-localization of *PLD2*-generated PA and VE-cadherin at cell-cell adhesion junctions. Inhibition of *PLD2* activity resulted in prolonged phosphorylation of Tyr-658 in VE-cadherin during the recovery phase 3 h post-thrombin challenge. Immunoprecipitation experiments revealed that after HLMVECs are thrombin stimulated, *PLD2*, VE-cadherin, and protein-tyrosine phosphatase nonreceptor type 14 (PTPN14), a *PLD2*-dependent protein-tyrosine phosphatase, strongly associate with each other. PTPN14 depletion delayed VE-cadherin dephosphorylation, reannealing of adherens junctions, and barrier function recovery. *PLD2* inhibition attenuated PTPN14 activity and reversed PTPN14-dependent VE-cadherin dephosphorylation after thrombin stimulation. Our findings indicate that *PLD2* promotes PTPN14-mediated dephosphorylation of VE-cadherin and that redistribution of VE-cadherin at adherens junctions is essential for recovery of endothelial barrier function after an edemagenic insult.

Increased lung vascular permeability is a defining feature and hallmark of acute lung injury (ALI), and is characterized by severe hypoxemia and alveolar flooding. Despite improved understanding of ALI pathophysiology, effective therapies to minimize the profound vascular leakage in ALI are not cur-

rently available and significant morbidity and mortality in critically ill patients is a major clinical problem. Vascular endothelial cell (EC) barrier function and integrity, critical for maintaining vascular homeostasis, depends on assembly of highly specialized transmembrane tight and adherens junction proteins including claudin, occluding, and vascular endothelial (VE)-cadherin (1–4). Among these transmembrane proteins, VE-cadherin is specifically and exclusively expressed in ECs, and it is a major regulator of vascular permeability changes and restoration of barrier integrity in response to barrier disruptive agents. Two potential mechanisms involving VE-cadherin internalization and tyrosine phosphorylation at Tyr-685 have been implicated in barrier disruption (5–8), whereas VE-cadherin recycling to adherens junctions (AJs) and dephosphorylation of tyrosine-phosphorylated VE-cadherin facilitates junctional reannealing and restoration of barrier function. Besides tyrosine phosphorylation, serine phosphorylation at Ser-665 in VE-cadherin also has been shown to modulate AJ assembly (9, 10). Tyrosine phosphorylation of VE-cadherin at Tyr-685 leads to the dissociation of catenin from VE-cadherin, and several kinases including c-Src, focal adhesion kinase, and p21-activated kinase have been described to play a role in VE-cadherin phosphorylation *in vivo* and/or *in vitro* (7, 10–13). As dephosphorylation of VE-cadherin is essential for restoration of AJs and barrier function, several protein-tyrosine phosphatases (PTPs) have also been shown to dephosphorylate tyrosine-phosphorylated VE-cadherin (14–16). Among the PTPs, VE-PTP is the most investigated phosphatase associated with regulation of VE-cadherin dephosphorylation and endothelial permeability (17). Other phosphatases, such as PTP1B, PTP2A, SHP2, DEP-1, RPTP- μ , have also been shown to regulate VE-cadherin phosphorylation (17). Recently a nonreceptor PTP, PTPN14, also known as PTPD2, PEZ, or PTP36, belonging to the class I PTP family containing an N-terminal noncatalytic domain, similar to that of band 4.1 superfamily cytoskeleton-associated proteins, was reported (18, 19). Deficiency or loss of PTPN14 resulted in developmental defects and lymphedema in mice and humans (20, 21), and there is evidence that mutations of PTPN14 are associated with cancers (22, 23). However, the biological functions of PTPN14 and its target(s) remain

* For correspondence: Viswanathan Natarajan, visnatar@uic.edu.

PLD2 regulation of barrier restoration via PTPN14 in endothelium

poorly characterized. A recent study has demonstrated that the lipid second messenger, phosphatidic acid (PA), binds to PTPN14 *in vitro* and enhances its catalytic activity, and this interaction was implicated in mammary epithelial cell morphogenesis (24). Very little is known on the role of PTPN14 in endothelial function and barrier regulation.

PA is a bioactive phospholipid generated either from glycerol 3-phosphate or dihydroxyacetone phosphate during *de novo* biosynthesis of phospholipids (25), and also generated by phospholipase D (PLD)-mediated hydrolysis of phosphatidylcholine or other phospholipids in mammalian cells (26). There are six isoforms of PLD, PLD1–6, of which PLD1 and PLD2 have been widely recognized in several human pathophysiology including cancer, hypertension, neurodisorders, diabetes, and acute lung injury (27, 28). PLD-generated PA mediates a variety of cellular functions, including growth/proliferation (29, 30), vesicle trafficking (31, 32), cytoskeletal rearrangement (33–35), and activation of NADPH oxidase (36), and most of its functions are attributed to the broad interactions with other proteins and lipids. PLDs have been shown to interact with 58 proteins and 5 lipids, and PA was found to target 50 proteins (37). In this study we show for the first time that genetic deletion of PLD2 in mice exacerbates protease-activated receptor-1-activating peptide (PAR-1-AP), a peptide analog of thrombin, or lipopolysaccharide (LPS)-induced lung inflammation and injury *in vivo* and *ex vivo*. We provide evidence that VE-cadherin restoration at AJs and endothelial barrier recovery after stimulation by thrombin or LPS is regulated by PLD2/PA-activated PTPN14. PLD2/PA signaling facilitates recovery of thrombin- or LPS-induced endothelial permeability and VE-cadherin dephosphorylation at AJs post-thrombin challenge. Furthermore, the PA signal was found to accumulate at AJs concurrently with redistributed VE-cadherin, and PLD2 interacted with PTPN14 and VE-cadherin during endothelial barrier recovery and restoration of AJs in response to thrombin challenge. These results demonstrate that PLD2/PA signaling is essential for proper EC barrier recovery and PTPN14 is a novel PA-regulated PTP that mediates VE-cadherin de-phosphorylation and restoration at AJs.

Results

Genetic deletion of *Pld2* in mice accentuates PAR-1-activating peptide- and LPS-induced lung permeability and vascular leak

Activation of G protein-coupled PAR-1, a G protein-coupled receptor, by thrombin or PAR-1-AP (or simply referred to as PAR1) increases endothelial permeability and leads to endothelial dysfunction (38–40). Thrombin is a potent stimulator of human endothelial cell PLD (41, 42) and both basal and thrombin-induced PLD activity was shown to be reduced by the dominant-negative *mPld2* K758R mutant but not by the *hPLD1* K898R dominant-negative mutant (32). However, the role of PLD1 and PLD2 in thrombin-induced lung endothelial permeability and pulmonary leak *in vivo* is unknown. Therefore, we examined the effect of PAR-1-AP on mouse lung permeability and vascular leak using wildtype (WT), *Pld1*^{-/-}, and *Pld2*^{-/-} mice. Deletion of PLD1 and PLD2 protein expression in lung tissues of *Pld1* and *Pld2* knockout

mice, respectively, was confirmed as described (43). Intratracheal administration of PAR-1-AP induced accumulation of inflammatory cells, mainly neutrophils, in lung alveolar spaces in WT, *Pld1*, and *Pld2* knockout mice as visualized by hematoxylin and eosin staining of lung sections. However, *Pld2*^{-/-} mice showed greater neutrophil accumulation compared with WT and *Pld1*^{-/-} mice (Fig. 1, A and B). Furthermore, *Pld2*^{-/-} mice showed significantly higher bronchoalveolar lavage (BAL) fluid protein content (Fig. 1C), and a small but significant increase in the IL-6 level in BAL fluids compared with WT, and *Pld1*^{-/-} mice after a 3-h PAR-1-AP challenge (Fig. 1F) with no significant difference in BAL TNF α levels (Fig. 1G). The effect of PLD deficiency on PAR-1-AP-induced lung vascular leak was assessed *in vivo* by uptake of Evans blue dye conjugated to albumin as described (44). As shown in Fig. 1D, PAR-1-AP induced a much greater increase in Evans blue dye uptake in *Pld2*^{-/-} mice lungs as compared with WT or *Pld1*^{-/-} mice indicating significantly greater lung vascular leakage in response to PAR-1-AP in *Pld2*-deficient mice. Additionally, the effect of *Pld2* deficiency on pulmonary vascular capillary filtration coefficient (K_{fc}) was investigated (Fig. 1E). *Pld2*^{-/-} mice showed higher K_{fc} compared with WT mice, indicating PLD2 plays a critical role in maintaining pulmonary vascular barrier function.

Next, we determined the role of *Pld1* and *Pld2* in LPS-induced lung vascular permeability and inflammatory cell infiltration in the lungs of WT, *Pld1*^{-/-}, and *Pld2*^{-/-} mice. Interestingly, we observed that total BAL fluid protein and leukocyte counts at 6 h post-LPS challenge were similar between WT and *Pld2*^{-/-} mice; however, BAL fluid protein and leukocyte count remained persistently higher in *Pld2* knockout as compared with WT mice (Fig. 2, A–C). Similar to PAR-1-AP, LPS induced greater Evans blue dye uptake in *Pld2*^{-/-} mice compared with WT or *Pld1*^{-/-} mice at 24 h post-LPS challenge (Fig. 2D). Furthermore, *Pld2*^{-/-} mice showed higher levels of pro-inflammatory cytokines in BAL 24 h after LPS treatment (Fig. 2, E and F). Collectively, the *in vivo* and *ex vivo* data show that deletion of *Pld2* in mice enhanced lung vascular leakage and inflammatory injury in response to PAR-1-AP or LPS challenge.

1-Butanol, *mPld2* K758R mutant, and PLD2 inhibitor VU0364739 retard barrier recovery at adherens junctions

Having demonstrated a role for *Pld2* in PAR-1-AP and LPS-induced lung vascular leakage in mice, we next investigated PLD2/PA signaling in the regulation of thrombin- or LPS-induced endothelial permeability and VE-cadherin distribution in the cell periphery of human lung microvascular endothelial cells (HLMVECs) by transient inhibition of PLD2. In the first approach, we treated HLMVECs with 0.1% of 1-butanol for 1 h prior to thrombin challenge, as mammalian PLD1 and PLD2 not only catalyze hydrolysis of PC and other phospholipids to PA but also possess transphosphatidylase activity and generates phosphatidylbutanol instead of PA. This transphosphatidylation reaction is highly specific for short-chain primary alcohols, whereas secondary or tertiary short-chain alcohols do not serve as an acceptor of PA for the transphosphatidylation reaction in the presence of short-chain primary alcohol, such as 1-butanol,

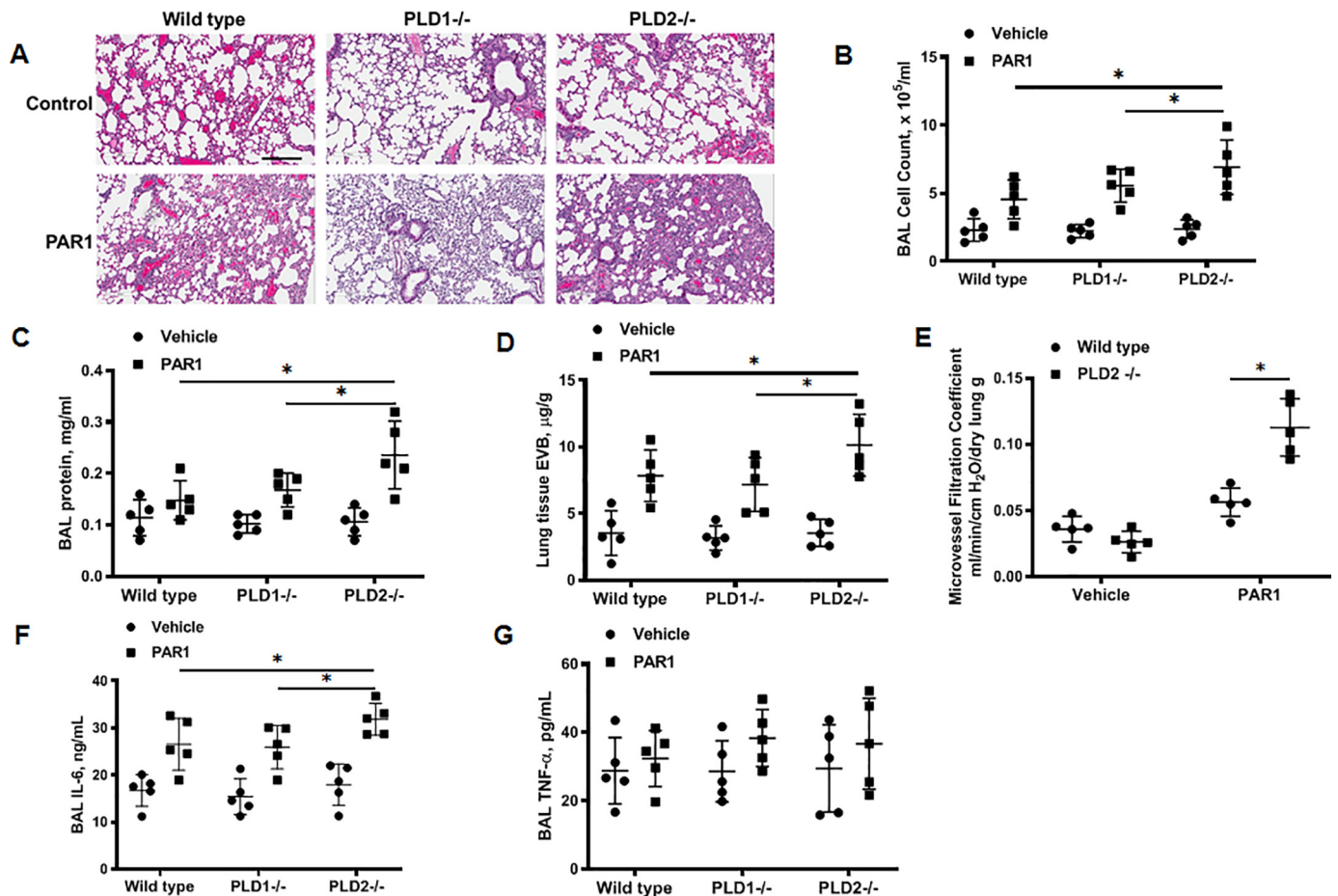


Figure 1. *Pld2*^{-/-} mice are more susceptible to protease-activated receptor activating peptide-induced pulmonary hyper-permeability. WT, *Pld1*^{-/-}, or *Pld2*^{-/-} knockout mice (*n* = 5 per group, both genders) were intratracheally challenged with either sterile PBS or PAR-1-AP (5 mg/kg) for 4 h. BAL was performed as described under “Experimental procedures,” *n* = 5. A, representative hematoxylin-eosin (H&E) staining of lung sections from WT, *Pld1*^{-/-} and *Pld2*^{-/-} with or without PAR-1-AP challenge. Original magnification ×10. BAL fluids were analyzed for infiltrating cells, protein, and pro-inflammatory cytokine levels. Scale bar = 200 µm. B, total infiltrated cells in BAL. *, *p* < 0.05, compared with WT or *Pld1*^{-/-} mice treated with PAR-1 agonist peptide. C, total protein levels in BAL fluid, *, *p* < 0.05 compared with WT or *Pld1*^{-/-} mice treated with PAR-1 agonist peptide. D, Evans blue dye accumulation in the lung tissue, *, *p* < 0.05, compared with WT or *Pld1*^{-/-} mice treated with PAR-1-AP. E, microvessel filtration coefficient measurement, *, *p* < 0.05, compared with WT mice treated with PAR-1-AP. F, BAL fluids pro-inflammatory cytokine IL-6 level, *, *p* < 0.01, compared with WT or *Pld1*^{-/-} mice treated with PAR-1 agonist peptide. G, TNF α level in BAL fluids in control and PAR-1-AP challenged WT and *Pld1*^{-/-} mice. Values between controls, *Pld1*^{-/-}, and *Pld2*^{-/-} mice were not significant.

but not secondary or tertiary short-chain alcohol, such as 3-butanol (Fig. 3A) (41). As shown in Fig. 3, B and C, 1-butanol, but not 3-butanol (0.1%, v/v), significantly reduced re-annealing of AJs and recovery of transendothelial electrical resistance (TER), a measurement of AJ integrity, following a thrombin-induced increase in endothelial permeability. The effect of PA on endothelial barrier function was further confirmed by immunofluorescence staining of VE-cadherin in cells exposed to thrombin, which revealed significant disruption of VE-cadherin at AJs in both 1-butanol- and 3-butanol-pretreated HLMVECs induced by thrombin challenge at 30 min. However, 3-butanol exposure, which does not affect PA production and PA-mediated signaling, allowed full recovery of VE-cadherin at AJs at 180 min, whereas 1-butanol, which acts as an acceptor of PA, impaired the recovery of VE-cadherin at AJs post-thrombin challenge (Fig. 3, D and E). These findings suggest that PA generation from either PLD1 or PLD2 or both may be involved in the signaling pathways that regulate endothelial barrier recovery at AJs.

As 1-butanol does not distinguish between PLD1 and PLD2, we overexpressed catalytically inactive adenoviral *hPLD1* and *mPld2* mutants, which function as dominant-negative mutants (32, 45) to reduce PLD activity. HLMVECs were infected with adenoviral control, *hPLD1*, or *mPld2* dominant-negative mutants for 48 h prior to thrombin challenge. As shown in Fig. 3, F and G, at 30 min of thrombin treatment, VE-cadherin staining showed obvious disruption at AJs. The AJs were re-established in cells infected with adenoviral control and *hPLD1* dominant mutant for 180 min, as indicated by VE-cadherin immunostaining. In contrast, *mPld2* dominant-negative mutant-infected cells failed to re-establish continuous AJs. In parallel experiments, inhibition of PLD2 with the specific inhibitor VU0364739 significantly reduced reannealing of AJs in thrombin-stimulated cells as determined by re-distribution of VE-cadherin (Fig. 3, H and I). A similar effect of blocking PLD2 with PLD2 inhibitor VU0364739 was observed with LPS-induced VE-cadherin distribution at AJs in HLMVECs (Fig. 3, J and K).

PLD2 regulation of barrier restoration via PTPN14 in endothelium

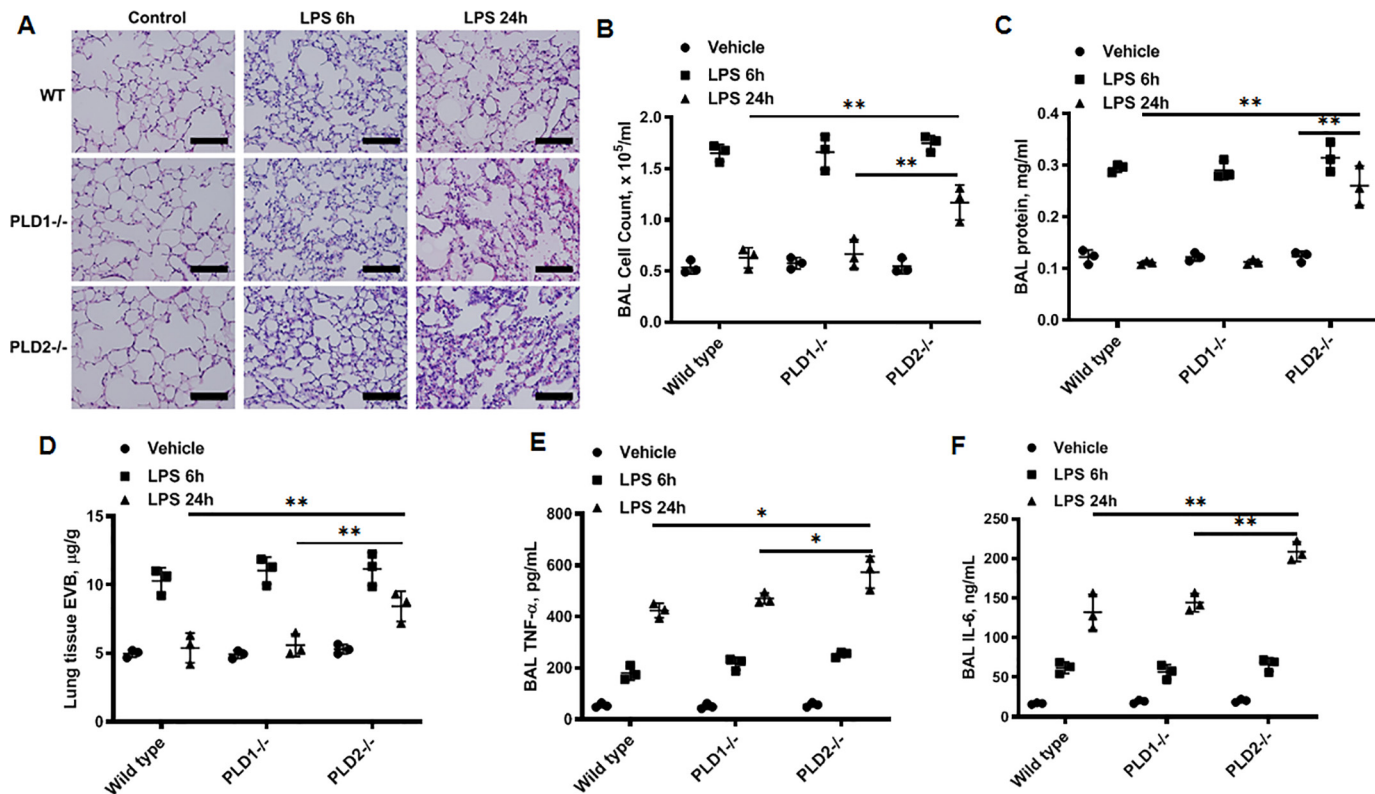


Figure 2. *Pld2*^{-/-} mice are more susceptible to LPS-induced acute pulmonary hyper-permeability. WT, *Pld1*^{-/-}, or *Pld2*^{-/-} knockout mice ($n = 3/\text{group}$ of both genders) were intraperitoneally treated with either sterile PBS or LPS for 6 or 24 h (10 mg/kg). BAL was performed as described under “Experimental procedures.” *A*, representative hematoxylin-eosin (H&E) staining of lung sections from WT, *Pld1*^{-/-}, and *Pld2*^{-/-} mice with or without LPS challenge. Original magnification $\times 20$. BAL fluids were analyzed for infiltrating cells, protein, pro-inflammatory cytokines levels. Scale bar = 100 μm . *B*, total infiltrated cells in BAL, **, $p < 0.01$, compared with WT or *Pld1*^{-/-} mice treated with LPS for 24 h. *C*, total protein levels in BAL fluid, **, $p < 0.01$, compared with WT or *Pld1*^{-/-} mice treated with LPS for 24 h. *D*, Evans blue dye accumulation in the lung tissue, **, $p < 0.05$, compared with WT or *Pld1*^{-/-} mice treated with LPS for 24 h. *E*, TNF α in BAL fluid, and *F*, IL-6 levels in BAL fluid. *, $p < 0.05$, compared with WT or *Pld1*^{-/-} mice treated with LPS for 24 h; **, $p < 0.01$, compared with WT or *Pld2*^{-/-} mice treated with LPS for 24 h.

Next, we investigated the effect of thrombin on VE-cadherin distribution in cell periphery of mouse lung microvascular endothelial cells (MLMVECs). As shown in Fig. 4, *A* and *B*, intensity of VE-cadherin in the cell periphery was significantly less in PLD2-deleted cells compared with the WT cells at 30 min post-thrombin stimulation. We also investigated the effect of ectopic expression of PLD2 on annealing AJs and recovery of barrier function in MLMVECs isolated from WT and *Pld2*^{-/-} mice. VE-cadherin redistribution to AJs in response to thrombin was significantly slower in MLMVECs isolated from *Pld2*^{-/-} mice and re-expression of PLD2 in *Pld2*^{-/-} cells enhanced restoration of VE-cadherin at AJs at 180 min post-thrombin stimulation (Fig. 4, *C* and *D*). The ecto-expression of PLD2 in WT and *Pld2*^{-/-} MLMVECs was verified by Western blotting of total cell lysates from adeno-control and adeno-PLD2 WT-infected cells (Fig. 4*E*). To address the functional relevance of PLD2 in endothelial barrier function, we determined endothelial barrier permeability responses by measuring TER in response to thrombin in MLMVECs deficient in *Pld2*^{-/-} and in cells infected with *Pld2* WT adenovirus. In *Pld2*-deficient cells, recovery of thrombin-induced TER was markedly slower compared with *Pld2* WT-infected cells (Fig. 4, *F* and *G*). Taken together, these data show that PLD2 and PLD2-derived PA are essential for recovery of endothelial permeability and VE-cadherin distribution at AJs after thrombin or LPS challenge of HLMVECs.

Spatio-temporal co-localization of PLD2 generated PA with VE-cadherin at AJs during barrier recovery in HLMVECs

PA is a bioactive phospholipid that interacts with a wide range of proteins to exert signal transduction and cellular functions (37). VE-cadherin is recycled to AJs in response to specific signaling cues (39, 40); therefore, we postulate that PLD2-generated PA is required for VE-cadherin trafficking to AJs during the onset of the recovery phase of endothelial barrier restoration as PA derived from PLD is involved in endocytic recycling and vesicle fusion (27, 32, 37, 46). This enables the formation of homotypic bonds to close inter-endothelial gaps and restore AJ barrier. To identify the role of PLD2-derived PA in VE-cadherin trafficking, we determined the spatio-temporal production of PLD2-generated PA in ECs using RFP-PASS, a recently developed PA biosensor (47, 48). As shown in Fig. 5*A*, in unstimulated HLMVECs, RFP-PASS was localized diffusely throughout the cytoplasm but upon stimulation with thrombin, it was translocated to the perinuclear found to be localized in vesicular structures prominent around the perinuclear vesicles, which started to occur at the area and the beginning of the restoration of AJs (60 min) after thrombin challenge (Fig. 5, *A* and *B*). Furthermore, PASS⁺ vesicles were significantly reduced by addition of 1-butanol (0.1%, v/v) but not 3-butanol (Fig. 5, *C* and *D*). Next, we investigated whether PLD2/PA mediates VE-cadherin re-distribution at AJs. HLMVECs were

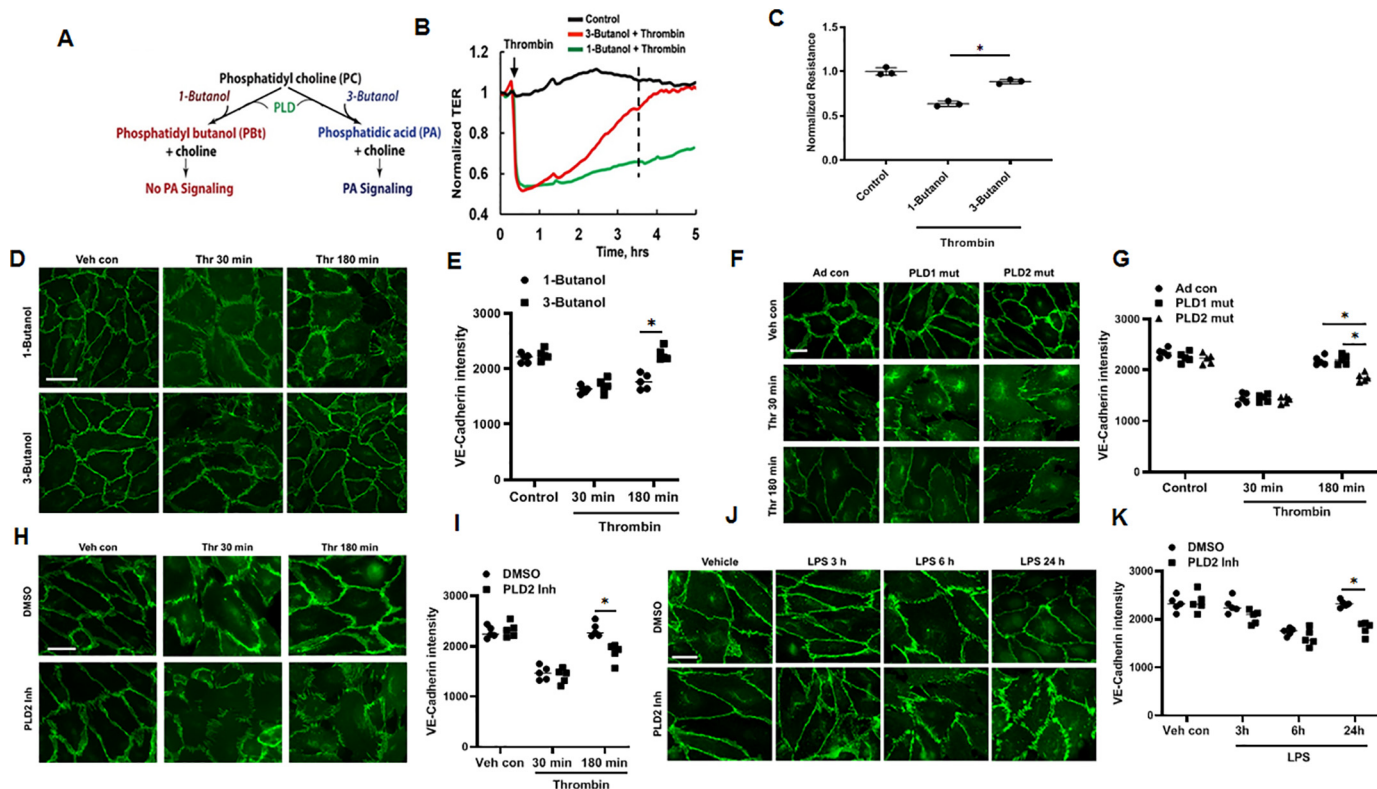


Figure 3. PA is critical for the restoration of impaired endothelial barrier function. *A*, assessment of PLD-PA signaling using primary (1-butanol) or tertiary alcohol (3-butanol). 1-Butanol modulates PLD-induced PA signaling by converting PA to PBT through transphosphatidylation reaction. In contrast, 3-butanol cannot transphosphatidylate PA to PBT and alter downstream signaling. *B*, HLMVECs grown on gold electrodes to ~90% confluence were pretreated with 1-butanol or 3-butanol (0.1% v/v) followed by 0.1 unit/ml of thrombin challenge. Real time changes in TER were measured, using ECIS, to assess endothelial barrier function. *C*, statistical analysis was performed at the time point outlined with a dashed line; normalized resistance data were obtained from 3 independent experiments. *D*, HLMVECs grown on slide chambers to ~90% confluence were pretreated with 1-butanol or 3-butanol (0.1%, v/v) for 1 h followed by 0.1 unit/ml of thrombin challenge for 30 or 180 min. Endothelial monolayer integrity was assessed by VE-cadherin immunofluorescent staining. Shown is a representative micrograph of three independent experiments. Scale bar = 10 μ m. *E*, VE-cadherin intensity in cell periphery from *D* was analyzed by ImageJ software. *, $p < 0.05$, compared with 1-butanol-pretreated cells. *F*, HLMVECs grown on slide chambers to ~90% confluence were infected with adenoviral vector control (25 MOI), *hPLD1* (25 MOI), or *mPld2* (25 MOI) dominant-negative mutant for 48 h prior to stimulation with thrombin (0.1 units/ml) for 30 or 180 min. Endothelial monolayer integrity was visualized by VE-cadherin immunofluorescent staining. Scale bar = 10 μ m. *G*, VE-cadherin intensity at the cell periphery was analyzed by ImageJ software. *, $p < 0.05$, compared with adenoviral control, adenoviral *hPLD1* or *mPld2* dominant-negative mutant-infected cells exposed to thrombin for 180 min. *H*, HLMVECs grown on slide chambers to ~90% confluence were pretreated with vehicle containing DMSO (1 μ M) or PLD2 inhibitor, VU0364739 (1 μ M in DMSO) for 1 h prior to 0.1 unit/ml of thrombin challenge for 30 or 180 min. Shown is a representative micrograph of three independent experiments. Endothelial monolayer integrity was visualized by VE-cadherin immunofluorescent staining. Scale bar = 10 μ m. *I*, VE-cadherin intensity was analyzed by ImageJ software. *, $p < 0.05$, compared with vehicle/DMSO-pretreated cells exposed to thrombin for 180 min. *J*, HLMVECs grown on slide chambers (~90% confluence) were pretreated with vehicle containing DMSO (1 μ M) or PLD2 inhibitor (1 μ M) for 1 h, as in *H*, followed by LPS (100 ng/ml) challenge for 3–24 h. Endothelial monolayer integrity was visualized by VE-cadherin immunofluorescent staining. Scale bar = 10 μ m. *K*, VE-cadherin intensity was analyzed by ImageJ software. At least 20 cells/area were analyzed for each condition, and results are representative of three independent experiments. *, $p < 0.05$, compared with vehicle/DMSO-pretreated cells exposed to LPS for 24 h.

co-infected with adenoviral GFP-tagged VE-cadherin and RFP-PASS plasmid to determine the dynamics of VE-cadherin and PA was investigated by live-cell imaging using confocal microscopy (Fig. 5, *E* and *F*). HLMVECs stimulated with thrombin showed increasing co-localization of RFP-PASS with GFP-tagged VE-cadherin at 60, 120, and 180 min post-thrombin challenge due to elevated generation of PA by PLD2, which coincides with the onset and completion of redistribution of VE-cadherin to AJs after endothelial barrier disruption (at 30 min of thrombin stimulation).

PLD2/PA signaling regulates of VE-cadherin dephosphorylation at Tyr-658

In AJs, VE-cadherin is maintained in a dephosphorylated state by PTPs, such as VE-PTP (14, 48) and SHP2 (49), whereas phosphorylation at Tyr-645, Tyr-658, Tyr-685, Tyr-731, and Tyr-733 by nonreceptor PTK including *c-Src* have been impli-

cated in AJ disassembly and loss of barrier integrity (50–52). Stimulation of HLMVECs with thrombin stimulated VE-cadherin Tyr-658 phosphorylation at 30 min, which returned to near basal phosphorylation status at 180 min post-thrombin challenge; however, the phosphorylation status at Tyr-685 and Tyr-731 after thrombin challenge were not significantly different from vehicle-treated cells (Fig. 6A). Based on this observation, we focused on VE-cadherin Tyr-658 phosphorylation in response to thrombin in all the experiments. To determine the role of PLD2 in regulating VE-cadherin Tyr-658 phosphorylation status, HLMVECs were infected with vector-control or dominant-negative *Pld2* mutant adenovirus (Fig. 6B) prior to stimulation with thrombin, and cell lysates were analyzed for VE-cadherin Tyr-658 phosphorylation. Thrombin stimulation of control cells infected with adenoviral vector alone showed transiently increased Tyr-658 VE-cadherin phosphorylation at 30 min, which returned to basal levels at 3 h post-thrombin

PLD2 regulation of barrier restoration via PTPN14 in endothelium

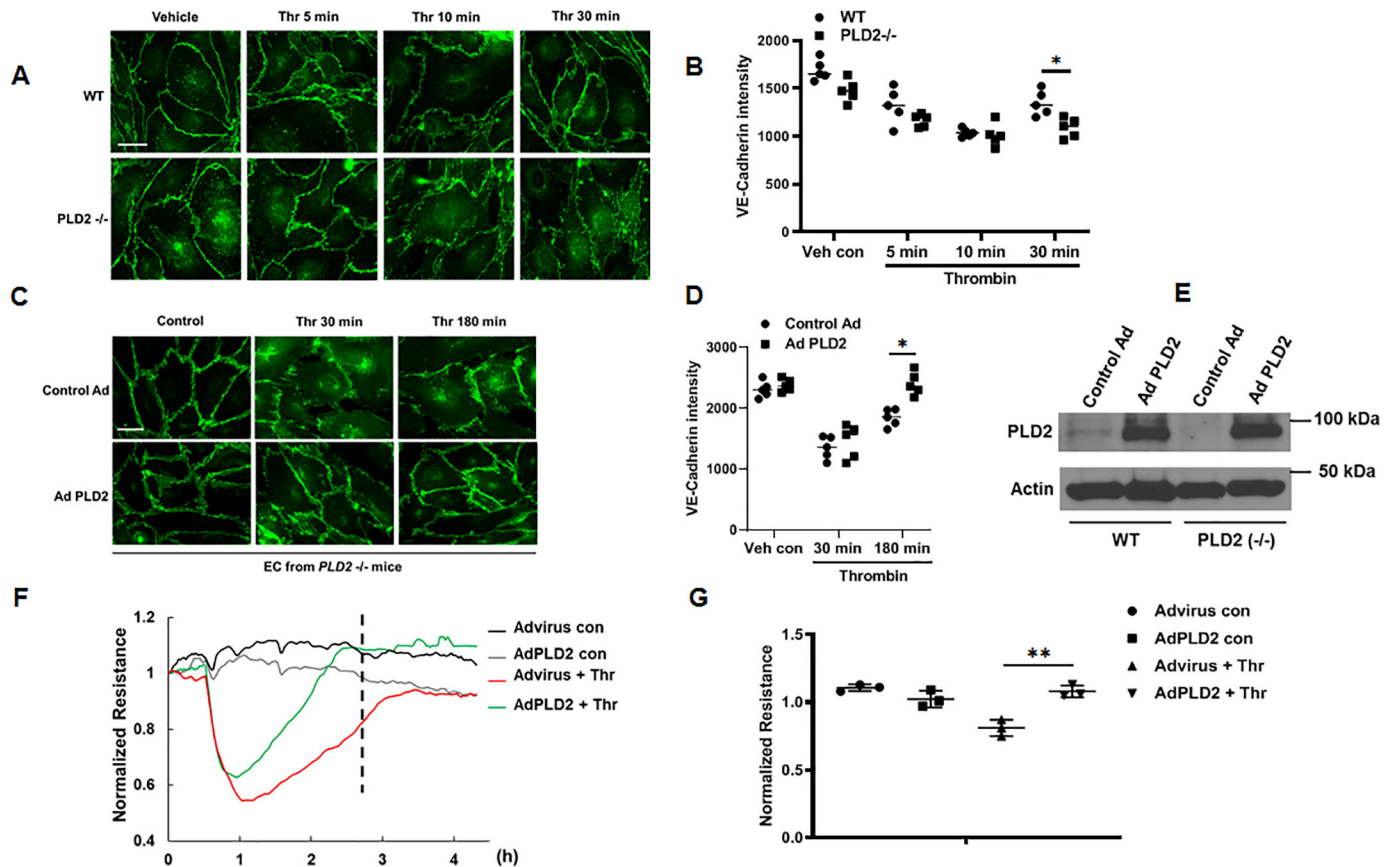


Figure 4. PLD2 is essential for thrombin-induced endothelial barrier function restoration. *A*, mouse lung endothelial cells isolated from WT or *Pld2* knockout mice were treated with thrombin (0.1 units/ml) for the indicated time periods, and the monolayer integrity was visualized by immunofluorescence staining for VE-cadherin. Representative images are shown. Scale bar = 10 μ m. *B*, VE-cadherin intensity was quantified by ImageJ software. *, $p < 0.05$, different from WT cells treated with thrombin for 30 min. *C*, mouse lung endothelial cells from *Pld2* knockout mice were infected with adenoviral vector control or adenoviral *mPld2* WT (25 MOI for 48 h) prior to thrombin (0.1 units/ml) challenge for 30 and 180 min. VE-cadherin distribution in cell junctions was assessed by immunofluorescence. Representative images are shown. Scale bar = 10 μ m. *D*, VE-cadherin intensity at cell junctions was quantified by ImageJ software and data are from three independent experiments in triplicate. *, $p < 0.05$, different from adenoviral vector control cells stimulated with thrombin. *E*, mouse lung endothelial cells isolated from WT and *Pld2*^{-/-} mice were grown on 35-mm dishes to ~70% confluence. Cells were infected with adenoviral vector control or adenoviral *mPld2* WT (25 MOI) for 48 h and cell lysates were subjected to SDS-PAGE and Western blotted for PLD2 with anti-PLD2 antibody. Shown is a representative blot of three experiments. *F*, HLMVECs grown on gold electrodes to ~80% confluence were infected with adenoviral vector control or adenoviral *mPld2* WT (25 MOI) for 48 h prior to stimulation with thrombin (0.1 units/ml). HLMVEC monolayer permeability dynamics were assessed by TER measurements carried out using ECIS. Shown is a representative tracing of three independent experiments in triplicate. *G*, statistical analysis of data from *F* was performed at the time point outlined with a line, using ANOVA. **, $p < 0.01$, compared with control adenoviral-infected cells exposed to thrombin.

challenge, whereas overexpression of the dominant-negative *Pld2* mutant resulted in sustained Tyr-658 phosphorylation of VE-cadherin (Fig. 6, *C* and *D*). This result suggests that reduced PA production from PLD2 sustains VE-cadherin Tyr-658 phosphorylation, compared with control cells, which is responsible for the delayed restoration of AJs. Similar observations of sustained VE-cadherin Tyr-658 phosphorylation were found in MLMVECs isolated from WT and *Pld2*^{-/-} mice. MLMVECs isolated from WT and *Pld2*^{-/-} mice were first challenged with vehicle or vehicle plus LPS for 6, 12, and 24 h, then cell lysates were analyzed for VE-cadherin Tyr-658 phosphorylation. As shown in Fig. 6, *E* and *F*, in cells from WT mice, LPS challenge enhanced Tyr-658 phosphorylation at 6 and 12 h, which returned to basal level at 24 h post-LPS treatment. In contrast, the LPS-induced Tyr-658 phosphorylation was sustained through 24 h in cells isolated from *Pld2*^{-/-} mice. These data agree with the impaired recovery of AJs observed in HLMVECs treated with PLD2 inhibitor prior to LPS challenge (Fig. 3). Together, these results suggest a key role for PLD2/PA signal-

ing as an upstream regulator of VE-cadherin Tyr-658 dephosphorylation in AJs.

Depletion of PTPN14, a PA-dependent PTP, retards VE-cadherin reannealing at AJs and recovery of barrier

Having demonstrated a key role for PLD2-generated PA in VE-cadherin Tyr-658 phosphorylation/dephosphorylation status after thrombin stimulation of HLMVECs or LPS challenge in MLMVECs, next we investigated the role of PTPN14, a PLD2/PA-dependent PTP, in VE-cadherin dephosphorylation following thrombin stimulation. A recent study identified the regulation of PTPN14 by PLD2-mediated production of PA in the stimulation of ERBB2 signaling in mammary epithelial MCF10A cells (24). To investigate the role of PTPN14 in endothelial barrier function, HLMVECs were transfected with scrambled or PTPN14 siRNA. Depletion of endogenous PTPN14 with PTPN14 siRNA significantly reduced VE-cadherin redistribution to AJs 180 min after thrombin treatment compared with scrambled siRNA-transfected HLMVECs

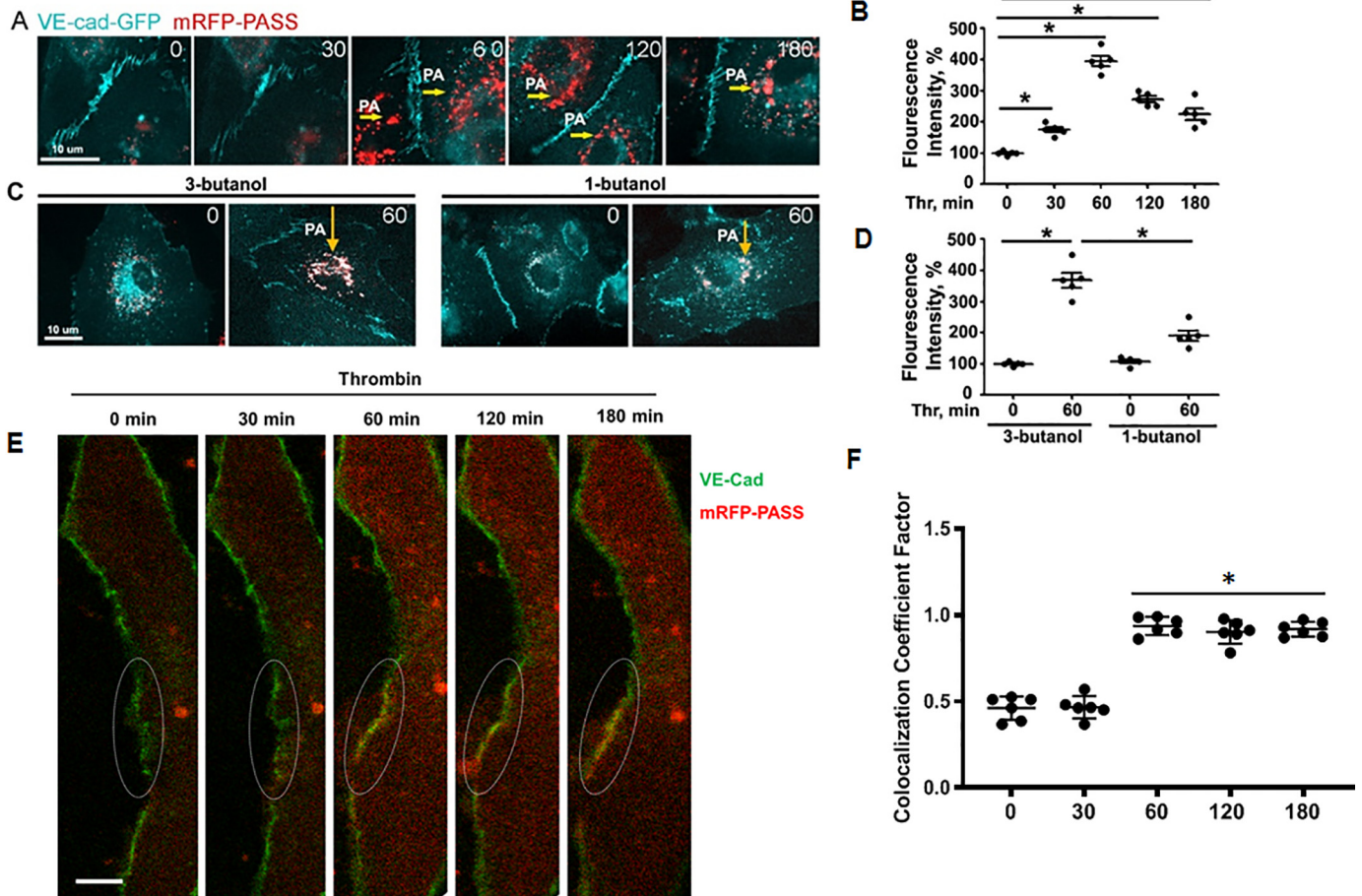


Figure 5. Thrombin induces spatio-temporal generation of PA and its co-localization with VE-cadherin at the onset of endothelial barrier recovery. *A*, HLMVECs grown in glass-bottom dishes (~70% confluence) were transfected with Lipofectamine reagent containing mRFP-PASS PA biosensor (5 μ g plasmid DNA) for 48 h as per the manufacturer's instruction, and then cells were treated with thrombin (0.1 units/ml). Images were acquired at the indicated time points. PA generation is indicated by arrows. Scale bar = 10 μ m. *B*, PASS fluorescent intensity was quantified as % increase in intensity, *, $p < 0.01$, compared with the 0 time point. *C*, HLMVECs were transfected with mRFP-PASS PA biosensor for 48 h, cells were treated with 1-butanol or 3-butanol prior to thrombin treatment. Images were acquired 60 min after thrombin treatment. Scale bar = 10 μ m. *D*, quantification of PA generation as fluorescence intensity percentage change. *, $p < 0.001$, compared with 3-butanol-treated control cells, or with 3-butanol-treated cells stimulated with thrombin for 60 min. *E*, HLMVECs were co-transfected with GFP-tagged VE-cadherin adenovirus and mRFP-tagged PA biosensor. Cells were treated with thrombin, and live cell imaging was acquired at the indicated time points. Scale bar = 10 μ m. *F*, co-localization of VE-cadherin and PA biosensor at the adherens junction area was quantified as co-localization of coefficient factor as described under "Experimental procedures," *, $p < 0.05$, as compared with the 0-min time point.

(Fig. 7, *A* and *B*). To further define the role of PTPN14 in thrombin-induced VE-cadherin phosphorylation/dephosphorylation, HLMVECs were transfected with scrambled or PTPN14 siRNA before thrombin treatment. Depletion of PTPN14 by siRNA attenuated thrombin-induced dephosphorylation of VE-cadherin at Tyr-658 at 180 min as compared with scrambled siRNA-transfected HLMVECs (Fig. 7*C*). A similar effect on VE-cadherin distribution at AJs and Tyr-658 VE-cadherin dephosphorylation was observed in HLMVECs transfected with the PTPN14 mutant plasmid that lacks activity when expressed (Fig. 7*D*). The functional role for PTPN14 in endothelial barrier function was further investigated by measuring TER. HLMVECs transfected with the scrambled siRNA showed relatively faster barrier recovery, whereas depletion of PTPN14 with siRNA prolonged the recovery process (Fig. 7, *E* and *F*). These results indicate PTPN14 plays a role in VE-cadherin redistribution to AJs and endothelial barrier recovery after thrombin stimulation.

Inhibition of PLD2 attenuates PTPN14 activity and reverses PTPN14-dependent VE-cadherin dephosphorylation after thrombin stimulation

Having established a key role for PLD2 and PTPN14 in thrombin-induced VE-cadherin distribution and phosphorylation/dephosphorylation at AJs, we next investigated the potential link between PLD2-dependent PA generation and the activation of PTPN14 in HLMVECs before and after thrombin stimulation. HLMVECs were transfected with FLAG-tagged PTPN14 WT plasmid for 48 h prior to treatment with PLD2 inhibitor and thrombin stimulation. Cell lysates were subjected to immunoprecipitation with anti-PTPN14 antibody and immunoprecipitates were assayed for PTPN14 activity using a commercial PTP activity assay kit. As shown in Fig. 8*A*, transfected cells showed enhanced expression of FLAG-PTPN14, and stimulation with thrombin decreased PTPN14 activity at 30 min, which was restored at 180 min post-thrombin challenge. Inhibition of PLD2 with a specific PLD2 inhibitor

PLD2 regulation of barrier restoration via PTPN14 in endothelium

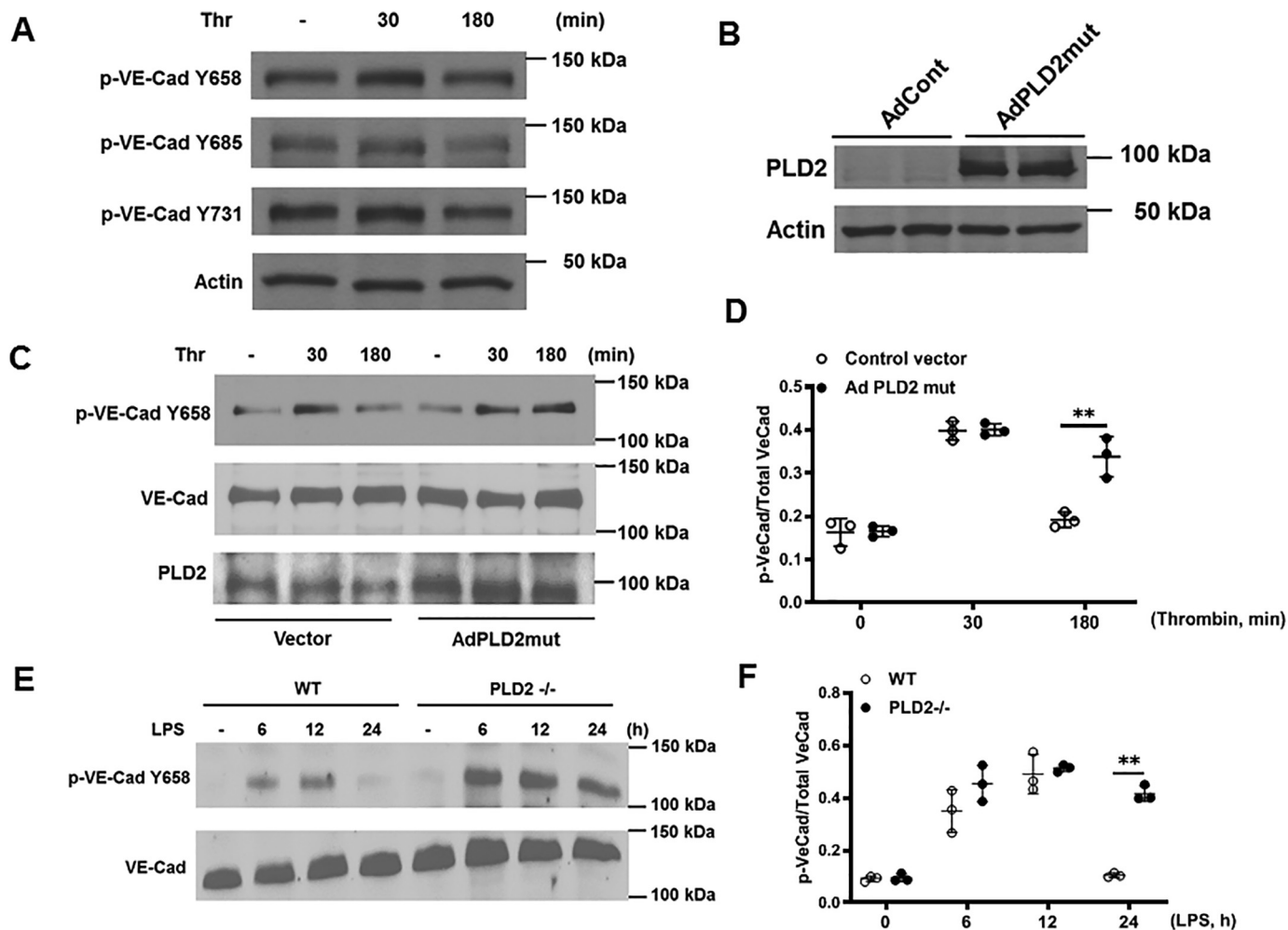


Figure 6. PLD2 mediates dephosphorylation of VE-cadherin for adhesion junction restoration. *A*, HLMVECs of ~90% confluence were treated with vehicle or thrombin (0.1 unit/ml) for 30 and 180 min. Cell lysates (20 μ g of protein) were subjected to SDS-PAGE, and membranes were probed with VE-cadherin Tyr-658, Tyr-685, and Tyr-731 phosphoantibodies. Shown is a representative blot from three independent experiments. *B*, HLMVECs (~60% confluence) were infected with adenoviral vector control or *mPld2* dominant-negative mutant (25 MOI) for 48 h and cell lysates were subjected to SDS-PAGE for expression of PLD2 protein by Western blotting and anti-PLD2 antibody. A representative blot is shown. *C*, HLMVECs (~60% confluence) were infected with adenoviral vector control or *mPld2* dominant-negative (25 MOI) for 48 h prior to stimulation with thrombin (0.1 unit/ml) for 30 and 180 min. Cell lysates (20 μ g of protein) were subjected to SDS-PAGE and membranes were probed with anti-VE-cadherin Tyr-658, anti-VE-cadherin, or PLD2 antibodies. Shown is a representative blot from three independent experiments. *D*, quantification of phosphorylation of VE-cadherin Tyr-658 from *C*, by densitometry and ImageJ analysis. Values are presented as ratio of phosphorylated VE-cadherin intensity to total VE-cadherin intensity. **, $p < 0.005$, compared with control vector-infected cells treated with thrombin. *E*, mouse lung endothelial cells isolated from either WT or *Pld2* knockout mice were treated with LPS (100 ng/ml) for the indicated time periods. Cell lysates (20 μ g of protein) were subjected to SDS-PAGE and phosphorylation of VE-cadherin at Tyr-658 was analyzed by Western blotting. Shown is a representative blot from three independent experiments. *F*, quantification of phosphorylated VE-cadherin Tyr-658 and presented as the ratio of phosphorylated protein intensity to total protein intensity, **, $p < 0.001$, compared with WT cells treated with LPS for 24 h.

decreased PTPN14 activity in the immunoprecipitates at 30, 60, 180 min post-thrombin treatment (Fig. 8B). Interestingly, in control cells not treated with PLD2 inhibitor, PTPN14 activity was reduced at 30 min after thrombin stimulation and returned to near control levels at 180 min post-thrombin treatment (Fig. 8B). The role of PLD2 in PTPN14 activation was further investigated in HLMVECs transfected with PTPN14 WT plasmid prior to treatment with PLD2 inhibitor and thrombin stimulation. Ecto-expression of PTPN14 reduced thrombin-mediated VE-cadherin Tyr-658 phosphorylation at 30 min, whereas inhibition of PLD2 with the specific inhibitor prolonged VE-cadherin Tyr-658 dephosphorylation at 180 min post-thrombin challenge (Fig. 8C). Furthermore, inhibition of PLD2 in PTPN14 over-expressing cells showed higher basal VE-cadherin Tyr-658 phosphorylation and prolonged VE-cadherin Tyr-658 phosphorylation

after exposure of the cells to thrombin (Fig. 8D). These results further support the role of PLD2/PA signaling in PTPN14-dependent VE-cadherin Tyr-658 dephosphorylation in response to thrombin in HLMVECs.

Thrombin increases association of PLD2, PTPN14, and VE-cadherin in HLMVECs

Based on the above results, we hypothesized that an increase in association between PLD2, PTPN14, and VE-cadherin after thrombin stimulation could facilitate VE-cadherin dephosphorylation at AJs and thereby endothelial barrier recovery. This was tested by a series of immunoprecipitation experiments to determine potential interactions between PLD2, PTPN14, and VE-cadherin. In three independent experiments, after stimulation with vehicle or thrombin for 30, 60, and 180 min,

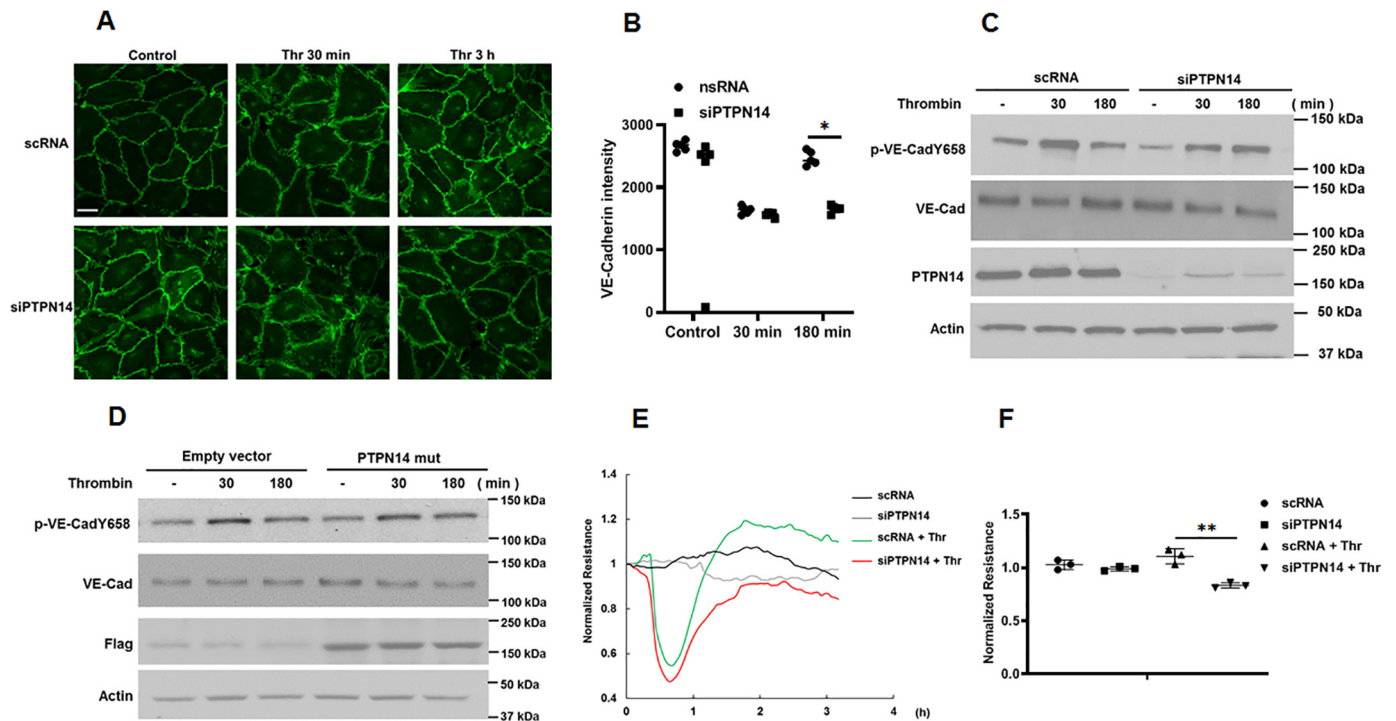


Figure 7. PA-dependent PTPN14 plays a critical role in determining VE-cadherin dephosphorylation and reannealing at adhesion junctions. *A*, endogenous PTPN14 in HLMVECs was down-regulated by siPTPN14 siRNA transfection, cells were treated with thrombin (0.1 unit/ml) for 30 or 180 min and then subjected to immunofluorescent staining of VE-cadherin for visualization of adhesion junctions' integrity. Scale bar = 10 μ m. *B*, statistical analysis of VE-cadherin intensity, *, $p < 0.05$, compared with scrambled siRNA-transfected cells treated with thrombin (0.1 unit/ml) for 180 min. (●, scRNA; ■, siPTPN14). *C*, in a parallel experiment, phosphorylation of VE-cadherin at Tyr-658 was assessed by Western blotting. A representative blot is shown. *D*, to explore whether PTPN14 activity is required for VE-cadherin dephosphorylation, HLMVECs were transfected with either empty vector plasmid or PTPN14 dominant-negative mutant plasmid. Phosphorylation of VE-cadherin at Tyr-658 was assessed by Western blotting. A representative blot is shown. *E*, HLMVECs were transfected with either scrambled or PTPN14 siRNA, 48 h after transfection cells were re-seeded onto an 8-well ECIS plate. After formation of monolayer, cells were treated with vehicle or thrombin (0.1 unit/ml), and TER was monitored. *F*, statistical analysis was performed at the time point 2 h, **, $p < 0.01$, compared with scrambled RNA-transfected cells exposed to thrombin. (●, scRNA; ■, siPTPN14; ▲, scRNA + thrombin; ▼, siPTPN14 + thrombin.)

HLMVEC lysates were subjected to immunoprecipitation. In immunoprecipitates of cell lysates with a VE-cadherin antibody, we found co-immunoprecipitation of PTPN14 with VE-cadherin under basal conditions; thrombin treatment caused a temporary dissociation of PTPN14 from VE-cadherin, which was restored to near basal levels (Fig. 9, *A* and *B*). Furthermore, PLD2 was also co-immunoprecipitated along with VE-cadherin, and the interaction was enhanced at 120 and 180 min post-thrombin treatment (Fig. 9, *A* and *B*). In contrast, there was no significant co-immunoprecipitation of PLD1 or change in PLD1 level, as compared with PLD2, in VE-cadherin immunoprecipitates in the presence or absence of thrombin challenge (Fig. 9*A*). Similarly, VE-cadherin co-immunoprecipitated in cell lysates were subjected to immunoprecipitation with PTPN14 (Fig. 9, *C* and *D*), and PLD2 (Fig. 9, *E* and *F*) antibodies, respectively, at 120 and 180 min post-thrombin challenge. Next, we sought to investigate whether PLD2 activity is required for the interaction between VE-cadherin and PTPN14. To this end, HLMVECs were pre-treated with DMSO or PLD2 inhibitor followed by thrombin challenge. DMSO-treated cells showed significant interaction between VE-cadherin and PTPN14 during the barrier function recovery phase; however, PLD2 inhibitor-treated cells showed impaired association between VE-cadherin and PTPN14 (Fig. 9, *G* and *H*). Association between PTPN14 and VE-cadherin was further investigated in HLMVECs transfected with VE-cadherin and PTPN14

plasmids. After challenged with thrombin (30–180 min), co-localization of VE-cadherin (red) and PTPN14 (green) was visualized by immunofluorescence staining. As shown in Fig. 10*A*, there was significant co-localization between VE-cadherin and PTPN14 prior to thrombin addition, and stimulation with thrombin for 30 min decreased co-localization at the cell periphery (Fig. 10*B*). However, at 180 min post-thrombin challenge, the co-staining of VE-cadherin with PTPN14 was restored in the cell periphery (Fig. 10, *A* and *B*). Collectively, these results showed that PLD2, PTPN14, and VE-cadherin are associated in a complex during barrier disruption and recovery, and that PLD2 activity is essential for the association between VE-cadherin and PTPN14 in HLMVECs.

Discussion

Disassembly of AJs in lung endothelial cell monolayers by edemagenic agents causes microvascular hyper-permeability and protein-rich pulmonary edema formation, and if uncorrected, leads to deterioration of lung gas exchange and function (53, 54). Despite our current understanding of the multifaceted mechanisms regulating vascular permeability, little is known about the molecular regulation of endothelial barrier restoration following lung injury and edema. In this study, we show a protective role for PLD2 in PAR-1–AP and LPS-induced lung inflammation and injury in mice. Also, we report a novel mechanism for restoration of endothelial barrier function through

PLD2 regulation of barrier restoration via PTPN14 in endothelium

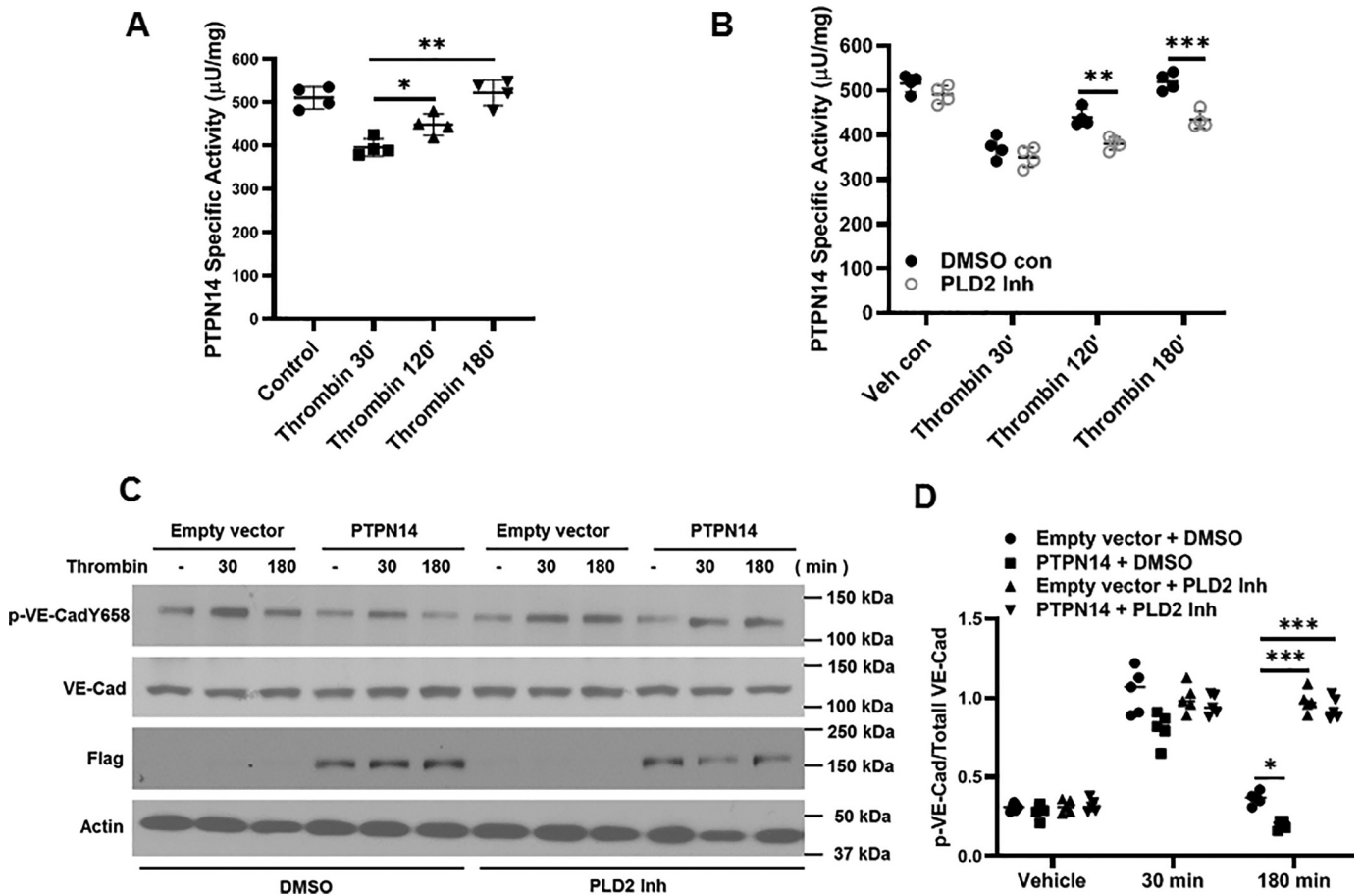


Figure 8. Thrombin induces transient decrease of PTPN14 activity followed by PLD2-dependent recovery of the activity during restoration of adhesion junctions. *A*, HLMVECs were treated with thrombin (0.1 unit/ml) for various times, cell lysates were incubated with anti-PTPN14 antibody to pull down PTPN14, and the immunoprecipitates were used for PTP activity assay with a commercial kit. *, $p < 0.05$, compared with thrombin 30 min; ***, $p < 0.005$, compared with thrombin for 30 min. (●, vehicle; ■, thrombin 30 min; ▲, thrombin 120 min; ▼, thrombin 180 min). *B*, HLMVECs were pretreated with PLD2 inhibitor (1 μM , 1 h) followed by thrombin (0.1 unit/ml) treatment for various time. PTPN14 activity measurement was carried out by immunoprecipitating pellets with PTPN14-specific antibody. **, $p < 0.01$, compared with DMSO control thrombin 120 min; ***, $p < 0.005$, compared with DMSO control thrombin 180 min. *C*, HLMVECs were transfected with either empty vector or FLAG-tagged WT PTPN14 plasmid for 48 h. Cells were then pretreated with DMSO (vehicle, 1 μl) or PLD2 inhibitor (1 μM in DMSO, 1 h) followed by thrombin (0.1 units/ml) treatment for 30 or 180 min. Cell lysates were collected and subjected to SDS-PAGE and Western blots were probed for VE-cadherin phosphorylation of VE-cadherin at Tyr-658, total VE-cadherin, FLAG, and actin with specific antibodies. A representative blot is shown. *D*, Western blots from *C* were quantified by densitometry and analysis by ImageJ and analyzed for statistical significance using ANOVA. *, $p < 0.05$ in cells transfected with FLAG-tagged PTPN14 and challenged with thrombin compared with vector control-transfected and thrombin-challenged cells; ***, $p < 0.005$, compared with cells transfected with empty vector or FLAG-tagged PTPN14 plasmid and incubated with PLD2 inhibitor and challenged with thrombin.

PLD2-generated PA in regulating VE-cadherin dephosphorylation and stabilization at AJs through PTPN14. Importantly, our results show that PLD2 is an essential component of VE-cadherin/PTPN14 complex formation, and generation of PA in a spatio-temporal manner is critical for maintaining VE-cadherin in a dephosphorylated state in AJs in a PTPN14-dependent manner in lung ECs.

PLD activation in cells results in generation of PA, which is recognized as a key lipid second messenger involved in a number of cellular responses, such as proliferation (29, 30), vesicular trafficking (31, 32), cytoskeletal reorganization (33–35), activation of NADPH oxidase (36), secretion of pro-inflammatory cytokines (55), neo-intima formation (56), and endothelial barrier function (58). Studies describing the role of PLD in regulating endothelial permeability were carried out *in vitro* using either bovine pulmonary artery (57) or human umbilical vein ECs (58). Here, we demonstrate for the first time a role for PLD1 and PLD2 in lung endothelial permeability and injury

using genetically engineered mice. Genetic deletion of PLD2 and to a lesser extent PLD1 in mice exacerbated PAR-1-AP and LPS-induced pulmonary edema and injury (Figs. 1 and 2). Our *in vivo* study also suggests that depletion of PLD2 actually delays the recovery of PAR-1-AP and LPS-induced endothelial permeability. *In vitro*, recovery of thrombin-induced endothelial permeability was delayed or inhibited by addition of 1-butanol, which is known to divert the PA generated by PLD to the primary alcohol, resulting in production of phosphatidylbutanol (PbT), thus rendering PA unavailable for modulating PA-dependent cellular targets (41, 45). To prove the validity of the 1-butanol effect, lung ECs were treated with PLD2 inhibitor or infected with dominant-negative *mPld2* K758R mutant, and we observed a delay in the recovery of thrombin-induced permeability and redistribution of VE-cadherin to AJs. Earlier studies have demonstrated that agonist-induced permeability changes in the endothelium are dependent on signaling pathways regulating $[\text{Ca}^{2+}]_i$, activation of Rac/Rho, nonmuscle MLCK, pro-

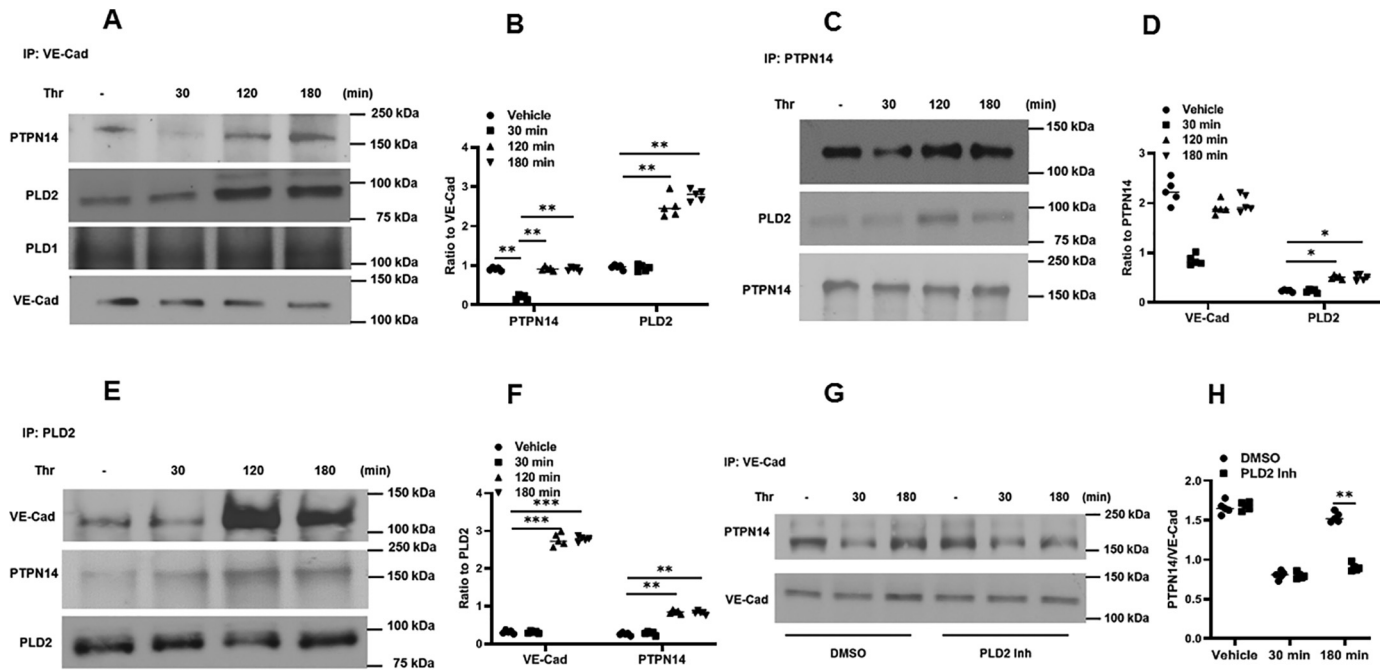


Figure 9. Thrombin induces formation of a signaling complex consisting of PLD2, PTPN14, and VE-cadherin. HLMVECs were treated with thrombin (0.1 unit/ml) for various times. Interactions between proteins were detected by immunoprecipitation assay with (A) VE-cadherin antibody, (C) PTPN14 antibody, and (E) PLD2 antibody. G, to investigate whether is PLD2 is required to interact between PTPN14 and VE-cadherin, HLMVECs were pretreated with PLD2 inhibitor (1 μ M, 1 h) followed by thrombin (0.1 units/ml) treatment for 30 or 180 min. Cell lysates were subjected to immunoprecipitation with VE-cadherin antibody to detect its interaction with PTPN14. Blots were quantified by densitometry and image analysis by ImageJ; B, **, $p < 0.01$, compared with vehicle control, thrombin 120 min, or thrombin 180 min. D, **, $p < 0.01$, compared with vehicle control, thrombin 120 min, or thrombin 180 min; *, $p < 0.05$, compared with vehicle control. F, ***, $p < 0.005$, compared with vehicle control; **, $p < 0.01$, compared with vehicle control. H, **, $p < 0.01$, compared with DMSO thrombin 180 min. ●, vehicle; ■, 30 min; ▲, 120 min; ▼, 180 min.

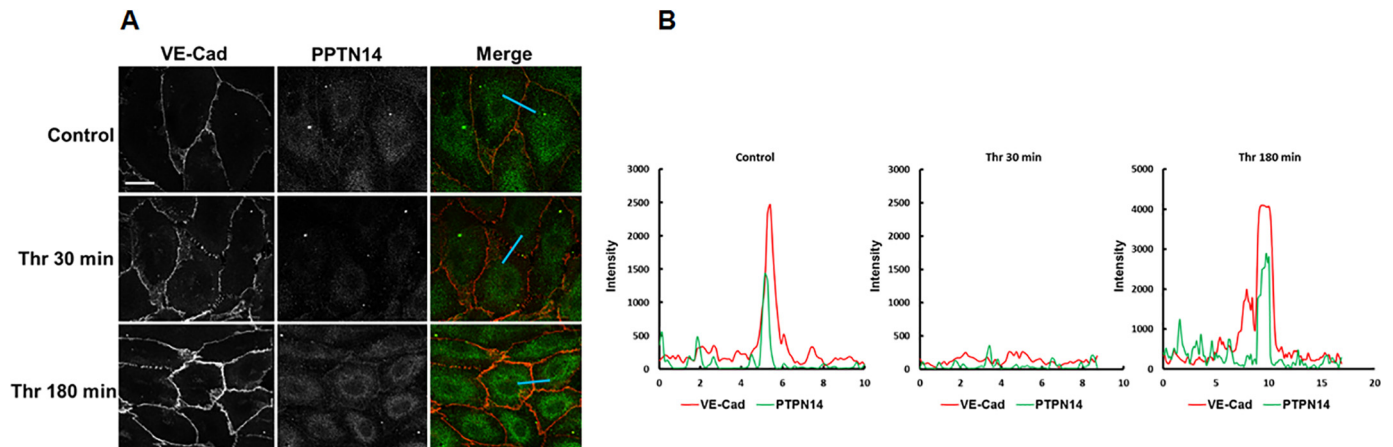


Figure 10. Thrombin induces dissociation of PTPN14 from VE-cadherin at adhesion junctions followed by a rapid re-association during the cell adhesion restoration phase. HLMVECs monolayer cultured on a glass-bottomed dish was challenged by thrombin treatment for 30 or 180 min. Co-localization of VE-cadherin (red) and PTPN14 (green) was visualized by immunofluorescent staining as described under "Experimental procedures." Scale bar = 10 μ m. B, a line across the cell periphery was drawn to plot each signal intensity along the line by ImageJ software and expressed as pixel intensity. At least 20 cells were analyzed for each condition, and results are representative of three independent experiments.

tein kinase C, Akt, mitogen-activated protein kinases, and Src kinases and there is considerable evidence that many of these pathways modulate the actin cytoskeleton, cell-cell adhesion junctions, and focal adhesions resulting in EC barrier disruption (57, 59–62). Although many of the studies have focused on mechanisms that regulate barrier disruption, a very few have addressed signaling pathways and cellular targets involved in AJ resealing and restoration of barrier integrity of the endothelium.

Our *in vivo* and *in vitro* results show that PLD2 is essential for the recovery of the endothelial barrier in response to thrombin

and LPS, and blocking PLD2/PA signaling attenuated redistribution of VE-cadherin to AJs. The role of PLD2 in restoration of VE-cadherin redistribution to AJs was validated using lung ECs isolated from *Pld2*^{-/-} mice wherein overexpression of adenoviral *Pld2* WT restored the redistribution of VE-cadherin to AJs after 180 min post-thrombin stimulation, which was similar to the VE-cadherin distribution pattern observed in cells from WT mice after thrombin challenge. VE-cadherin is an adhesive protein of endothelial junctions that forms *cis* and *trans* homophilic interactions to stabilize AJs between adjacent ECs (17). The adhesive function of VE-cadherin is attributed to phosphor-

PLD2 regulation of barrier restoration via PTPN14 in endothelium

ylation and dephosphorylation on tyrosine residues (14, 63, 64). Phosphorylation of VE-cadherin at tyrosine residues 658, 685, and 731 by inflammatory mediators, such as LPS, TNF α , and vascular endothelial growth factor, induced vascular permeability and leukocyte extravasation (14, 49, 65, 66). Furthermore, it has been shown that vascular permeability and leukocyte extravasation are regulated *in vivo* by phosphorylation of VE-cadherin at Tyr-685 and Tyr-731, respectively, suggesting differential regulation of endothelial functions by distinct tyrosine residues (8). Under our experimental conditions, thrombin preferentially stimulated VE-cadherin phosphorylation at Tyr-658 compared with 685 and 731 at 30 min of challenge suggesting a role for Tyr-658 phosphorylation in thrombin-induced barrier disruption. Tyrosine phosphorylation of VE-cadherin at 658 by *c-Src*, facilitates VE-cadherin internalization in a β -arrestin-dependent manner (3), and the internalized VE-cadherin enters endosomal compartments and is either recycled to the plasma membrane or subjected to degradation (67). Recent studies have shown that spatio-temporally generated PA from PLD2 acts as signaling platforms for MT1-MMP surface trafficking and lung metastasis of breast cancer cells (68), ERK signaling in cancer cells (47), podosome formation (69), and recruitment of IQGAP1 associated with neo-intima formation (56). In addition to PLD2, PLD1-mediated PA generation in microdomains promotes vesicular fusion to the plasma membrane during exocytosis of large dense-core granules (69); however, a role for PA confinement in microdomains in VE-cadherin redistribution to AJs is unknown.

In this study, we used a new PA biosensor, GFP/RFP-PASS to determine the role of PLD generated PA in VE-cadherin redistribution to AJs during endothelial recovery by live imaging. We found that VE-cadherin containing vesicles are enriched with the PA biosensor after thrombin stimulation and 1-butanol, but not 3-butanol, treatment of cells blocked VE-cadherin-RFP-PASS positive vesicles. Earlier, we demonstrated that PA generated by *RalA*-activated PLD2 stimulated caveolae-mediated endocytosis and vesicular trafficking in ECs (32). During AJ disassembly VE-cadherin is internalized in clathrin-coated vesicles that are enriched in specialized regions called clathrin-coated pits. These vesicles fuse with early endosomes containing VE-cadherin for recycling, and lysosomal or vesicular trafficking (65). Our preliminary study showed that stimulation with thrombin increased co-localization of Cav-1 with RFP-PASS or GFP-PLD2 in vesicles suggesting enrichment of VE-cadherin and PLD2 in Cav1 vesicles after thrombin stimulation (data not shown). Furthermore, studies are necessary to define the role for PLD1 and/or PLD2 in caveolae-mediated trafficking and VE-cadherin recycling to AJs.

In addition to regulation of VE-cadherin trafficking to AJs during the endothelial barrier recovery phase, we also observed that PLD2/PA signaling was involved in VE-cadherin dephosphorylation that is known to play a role in stabilization of AJs and resealing of the endothelial gaps after thrombin stimulation of HLMVECs. In the present study, we have shown that thrombin treatment caused dramatic disruption of VE-cadherin staining in AJs in association with a transient increase in Tyr-658 phosphorylation at 30 min, which was reversed to near

basal phosphorylation status at 180 min post-thrombin challenge. Furthermore, overexpression of the catalytically inactive *mPld2* mutant caused sustained phosphorylation of VE-cadherin at Tyr-658 suggesting that PLD2/PA signaling was regulating for VE-cadherin dephosphorylation post-thrombin challenge. Under our experimental conditions, the other two sites, Tyr-685 and Tyr-731, were not significantly phosphorylated by thrombin in HLMVECs. The phosphorylation status of VE-cadherin at Tyr-658 and other sites is regulated by protein-tyrosine kinase(s) and PTPs. *c-Src* (7) and PYK2 (64) have been shown to phosphorylate VE-cadherin, and promote AJ disassembly and endothelial permeability. PTPs that dephosphorylate tyrosine-phosphorylated VE-cadherin to stabilize endothelial AJs include β -catenin-associated SHP-2 (50), RPTP- μ (67), and VE-PTP (14). Of these three PTPs, the role of VE-PTP, an endothelial receptor-type tyrosine phosphatase, has been well studied. VE-PTP stabilizes AJs and endothelial barrier by supporting homotypic VE-cadherin adhesion and maintenance of low basal endothelial permeability (14, 15). Furthermore, VE-PTP counteracts the stimuli-induced endothelial permeability increase by enhancing VE-cadherin dephosphorylation at Tyr-658 and Tyr-685 leading to stabilization of VE-cadherin at AJs (14). However, recent studies show that VE-PTP also stabilizes VE-cadherin junctions and the endothelial barrier via a phosphatase-independent mechanism (66). Using the photoconvertible fluorescent protein VE-cadherin-Dendra2, it was shown that VE-PTP served as an adaptor protein that by binding and inhibiting the RhoGEF, GEF-H1 modulated Rho activity and tension across VE-cadherin junctions in quiescent endothelial monolayers (66). Thus, in resting cells VE-PTP regulated basal endothelial permeability independently of its enzymatic activity. Interestingly, blocking VE-PTP with antibodies or a pharmacological inhibitor, AKB-9778, or by gene ablation stabilizes endothelial junctions *in vivo* via a Tie-2 but VE-cadherin independent mechanism. In the absence of Tie-2, VE-PTP inhibition destabilized endothelial junctions suggesting a functional role for Tie-2 in barrier regulation in the absence of VE-cadherin (70). In this study, we identified a novel role for PTPN14, a PLD2-dependent nonreceptor PTP (24), in regulating thrombin-induced VE-cadherin stabilization in AJs in human lung ECs. Our study clearly demonstrates that the activity of PTPN14 is essential for stabilization of VE-cadherin at AJs through dephosphorylation of VE-cadherin during thrombin-induced endothelial barrier recovery of lung ECs. Transfecting HLMVECs with catalytically inactive PTPN14 mutant blocked VE-cadherin dephosphorylation during the recovery phase following thrombin challenge and prevented VE-cadherin stabilization at AJs. Furthermore, expression of the catalytically inactive PTPN14 mutant delayed the recovery of thrombin-induced permeability in HLMVECs compared with control cells. However, it is unclear if PTPN14 can stabilize VE-cadherin junctions and endothelial barrier independent of its phosphatase activity similar to that reported for inactive VE-PTP (14, 66). PTPN14 also exhibits phosphatase-independent functions, such as the ability to regulate Hippo signaling via direct interaction with YAP1 or with its upstream regulators, such as LATS1/2 and KIBRA, through PPXY motifs in PTPN14 (22). PTPN14 was identified as a major phosphatase of epithelial and

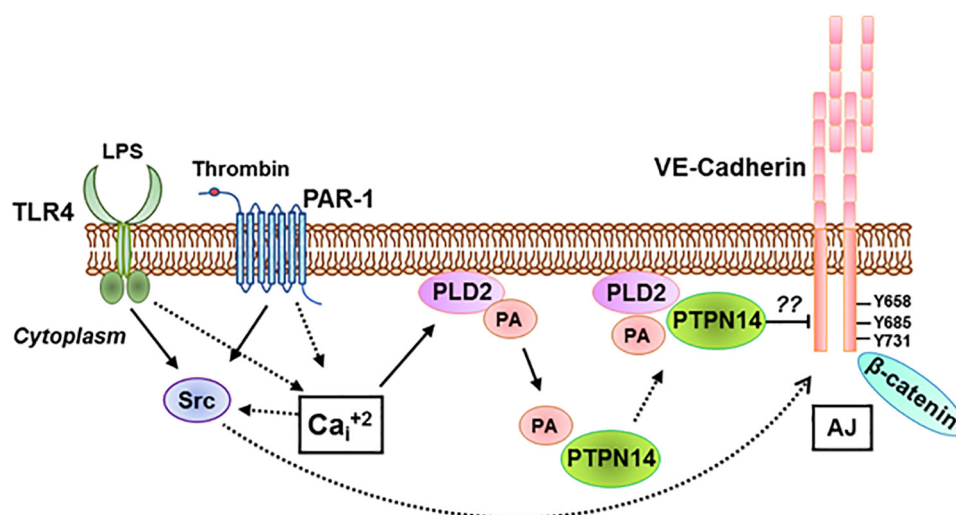


Figure 11. Model of PLD2/PA-regulated PTPN14 in VE-cadherin stabilization at endothelial AJs and barrier restoration. Stimulation of endothelial cells with LPS via Toll-like receptor (*TLR*) 4 or thrombin through protease-activated receptor-1 (*PAR-1*) results in changes in intracellular calcium, and Src activation. Changes in intracellular calcium and/or Src activation stimulates generation of PA mediated by PLD2 during the recovery phase of restoration of lung endothelial integrity. PA, a second messenger, activates PTPN14, and the activated PTPN14 maintains VE-cadherin at adherens junctions in a de-phosphorylated state resulting in re-annealing of AJs.

endothelial cell AJs and dominant-negative *PTPN14* (*Pez*) mutant enhanced cell motility suggesting potential regulation by PTPN14 through its action on cell-cell adhesion (18). Interestingly, PTPN14 is a positive regulator of ERBB2 signaling in mammary epithelial cells, which depends on PLD2-dependent (24), and in cancer cells PTPN14-promoted proliferation and migration through the regulation of Hippo/YAP signaling pathway (71). The contrasting effect of PTPN14 on cell motility between normal epithelial cells and gastric cancer cells is unclear but may be due to differences in the cell types and differential activation or inhibition of signaling pathways that regulate cell motility and proliferation. Interestingly, knock-down of *PTPN14* in HLMVECs by siRNA had no significant effect on thrombin-induced increased co-immunoprecipitation of PLD2 with VE-cadherin at 120 and 180 min post-thrombin challenge (data not shown), suggesting a nonrequirement of PTPN14 for the increased association between PLD2 and VE-cadherin.

In summary, our findings demonstrate a protective role of PLD2 in thrombin- and LPS-induced permeability and inflammatory lung injury in mice. We also show for the first time the involvement of PLD2-dependent PTPN14 in VE-cadherin dephosphorylation, redistribution to AJs, and recovery of barrier function after thrombin stimulation of lung ECs. Additionally, we provide evidence for interaction of PLD2, VE-cadherin, and PTPN14 in response to thrombin in lung ECs and how spatio-temporal generation of PA mediated by PLD2 is required for redistribution of VE-cadherin to AJs to promote endothelial barrier recovery (Fig. 11). It will be important to validate the role of PLD2 in activation of PTPN14 in regulating endothelial barrier function in animal models of lung injury. Thus, both PLD2 and PTPN14 could serve as novel therapeutic targets in regulating endothelial barrier function and restoration of stable AJs during lung inflammation and injury.

Experimental procedures

Materials

HLMVECs (catalogue no. cc-2583) and endothelial basal media (EBM-2) (catalogue no. 3162) were obtained from Lonza (San Diego, CA). Gold antifade mounting media (catalogue no. P36935), 4',6-diamidino-2-phenylindole, Hoechst and precast Tris glycine PAGE, Alexa Fluor 488 donkey anti-rabbit (A21026), Alexa Fluor 488 donkey anti-mouse (A21202), Alexa Fluor 568 goat anti-rabbit (A11036), Alexa Fluor 568 goat anti-mouse (A11037), and Alexa Fluor phalloidin 568 (A12380), were procured from Thermo Fisher Scientific, Waltham, MA). Hepatocyte growth factor (catalogue 315-23) was from Pepro-Tech (Rocky Hill, NJ). Antibody for phospho-VE-cadherin Tyr-658 (catalogue no. AB1955) was from Millipore Sigma. VE-cadherin (catalogue no. 160840) was purchased from Cayman Chemicals (Ann Arbor, MI). PLD1 (catalogue no. 3832), PLD2 (catalogue no. 13891) and cell lysis buffer (catalogue no. 9803) were from Cell Signaling Technology (Danvers, MA). FuGENE HD (catalogue no. E2311) transfection reagent was from Promega Corp. (Madison, WI). ECIS electrodes 8W1E were procured from Applied Biophysics (Troy, NY). RNA transfection reagent Gene Silencer (T500020) was from Genlantis (San Diego, CA). SU11274 (catalogue no. S1080) was purchased from Selleck Chemicals (Houston, TX). BSA (catalogue no. sc-2323) and *Pez* (F-12) (catalogue no. sc-373766) mouse monoclonal were obtained from Santa Cruz Biotechnology. Akt inhibitor VIII (catalogue no. ENZ-CHM125-0001) was from Enzo Life Sciences Inc. (Farmingdale, NY). Actin antibody (A15441) was from Abcam (Cambridge, UK).

Animal experiments with *PAR-1*-activating peptide

Age- and weight-matched male and female WT were anesthetized with ketamine as per the approved protocol and administrated a single intratracheal infusion of sterile PBS or *PAR-1*-AP (5 mg/kg body weight) for 4 h. After treatment, BAL

PLD2 regulation of barrier restoration via PTPN14 in endothelium

fluid was collected using 1 ml of sterile Hanks' balanced salt buffer, and differential cell counts were performed using cyto-spin. Cytokines and total protein in the BAL fluids were measured commercial kits. Left lungs were removed and fixed with 10% formalin, and paraffin-embedded 5- μ m thick sections were stained with hematoxylin and eosin for immunohistochemistry. The right lung was snap frozen in liquid nitrogen and stored at -80°C for total lysates, Western blots, and RNA. All mice were housed in the University of Illinois Animal Care Facility in accordance with institutional guidelines of the United States National Institutes of Health. All animal experiments were performed under the protocol approved by the Institutional Animal Care and Use Committee of the University of Illinois at Chicago.

Human lung endothelial cell culture

HLMVECs cultured in complete media (EBM-2) containing 10% fetal bovine serum (FBS), growth factors (provided as a kit from Lonza (San Diego, CA), and 1% penicillin/streptomycin were maintained at 37°C and 5% CO_2 and grown to contact-inhibited monolayers that revealed typical cobblestone morphology (72). Cells were then detached with 0.05% trypsin and resuspended in fresh complete EBM-2, and cultured on gold electrodes for electrical resistance determinations, on glass coverslips for fluorescent microscopy studies, or on 35-, 60-, or 100-mm culture dishes for preparation of cell lysates and Western blot analysis. Cells passaged from 4 to 8 were used in experiments.

Mouse lung endothelial cell isolation and culture

MLMVECs from age matched WT and *Pld2*^{-/-} mice were isolated using anti-mouse PECAM-1 antibody and Dynabeads M-450 (sheep anti-rat IgG) essentially as described (73). The cells were plated on Matrigel (BD Bioscience)-coated 35-mm dishes and allowed to grow to confluence in EGM-2 complete medium containing 10% FBS and growth factors provided as a kit by Lonza (San Diego, CA). Endothelial cells, passaged between 3 and 8, were used in experiments, and were characterized by their cobblestone morphology, PECAM-1 or CD31 expression, and Di-Ac-LDL uptake.

Transfection of siRNA

Depletion of endogenous PTPN14 and PLD2 in HLMVECs was carried out using gene-specific siRNA as described previously (74). In brief, pre-designed human PTPN14, PLD2 siRNA, or nonspecific/nontargeting siRNA were used to transfect HLMVECs (passage of 5–7). Before transfection, cells were starved in EBM-2 containing 2% FBS overnight and cells were transfected in EBM-2 serum-free media with 50 nM scrambled, PTPN14 or PLD2 siRNA complexed with the Gene Silencer transfection reagent according to the manufacturer's recommendation and incubated at 37°C for 4 h. At the end of the transfection period, the media was replaced with fresh complete EBM-2 supplemented with 10% FBS and growth factors, and cells were used 72 h post-transfection.

Immunoblotting and immunoprecipitation

Immunoblotting and immunoprecipitation (IP) were performed as described previously (74). In brief, after appropriate

treatments, cells were pelleted in ice-cold PBS, lysed in standard lysis buffer (Cell Signaling, Beverly, MA), and sonicated. Lysates were then centrifuged at $1,000 \times g$ for 10 min at 4°C , supernatants were collected, and protein assayed using BCA protein assay kit. For IP experiments, equal amounts of protein (1 mg) from each sample were pre-cleared with control IgG conjugated to A/G-agarose beads at for 1 h at 4°C , supernatants were collected and incubated overnight with primary antibody conjugated to A/G-agarose beads at 4°C . Next day, the samples were centrifuged at $1,000 \times g$ for 1 min in a Microfuge centrifuge and the pellet containing the agarose beads were washed three times with lysis buffer at room temperature. After centrifugation at $1,000 \times g$ for 1 min, the beads were collected by removing supernatant buffer, and 40 μ l of SDS sample buffer (100 mM Tris-HCl (pH 6.8), 4% SDS, 0.1% bromphenol blue, 20% glycerol, 200 mM DTT) were added to the beads and boiled. Lysates were then subjected to 10% SDS-PAGE followed by Western blotting. Proteins were detected by immunoblotting using appropriate primary antibodies, and horseradish peroxidase-conjugated anti-rabbit or anti-mouse secondary antibodies. Band intensities were quantified by densitometry using ImageJ software.

Measurement of endothelial permeability by transendothelial electrical resistance

The endothelial permeability changes were measured using the highly sensitive biophysical assay with an electrical cell impedance system (ECIS) (Applied Biophysics, Troy, NY) as described previously (72). The TER was measured dynamically across the monolayer, and the effect of thrombin challenge was monitored over a period of 6 h. Resistance was normalized to the initial voltage and expressed as a fraction of the normalized resistance value.

Immunofluorescence staining and quantification

Human lung HLMVECs were fixed with 3.7% formaldehyde at room temperature for 10 min and permeabilized with 0.1% Triton X-100 at room temperature for 10 min. After washing 3 times with PBS, cells were incubated with VE-cadherin antibody (1:100 in 2% BSA/PBS) at room temperature for 1 h. Cells were then rinsed 3 times with PBS and subsequently incubated with the respective secondary antibody conjugated with Alex Fluor-488/568 (1:2000 in 2% BSA/PBS) and Phalloidin 568 at room temperature for 1 h. Cells were then rinsed 3 times with PBS, coverslips were mounted with gold antifade mounting media containing Hoechst for 4',6-diamidino-2-phenylindole staining, and cells were examined under Nikon Microscope with $\times 60$ oil immersion objective and Meta Vue software. Quantification of VE-cadherin was performed by ImageJ software. Briefly, VE-cadherin at the cell-cell junction area was selected by segmentation function; the identified areas were used to generate regions of interest for quantification of fluorescence intensity.

Transfection and infection of ECs

GFP-PASS lentiviral construct was added to HLMVECs transfected with Cav-1-RFP for 48 h. Cells were then starved and stimulated with BSA (30 mg/ml). Adenoviral constructs,

vector control, and dominant-negative mutants of *hPLD1* K898R and *mPld2* K758R were generated at the University of Iowa Gene Transfer Vector Core (Iowa City, IA). Adenoviral constructs (25 pfu/cell) of Vector-control, *hPLD1* K898R, or *mPld2* K758R mutant were added to HLMVECs grown to ~80% confluence in EBM-2-MV growth media (Lonza) supplemented with 10% FBS. After overnight culture, the virus-containing medium was replaced with fresh complete medium.

TIRF microscopy

HLMVECs transfected with Cav-1-RFP were infected with adenoviral vector control, *hPLD1* K898R, or *mPld2* K758R mutants for 36 h and then starved for 3 h before stimulation. In some experiments, 200 nM PLD inhibitor was added into the system 1 h before stimulation. Live cell TIRF (total internal reflective fluorescence) images were acquired using a Zeiss Axio Observer. Z1 Microscope (Carl Zeiss MicroImaging, Inc.) with 561 nm excitation and a $\times 100/1.46$ NA α -Plan-Fluar objective. Experiments were conducted at 37 °C in 5% CO₂ in a Pecon XL TIRF S incubator chamber.

Quantification of co-localization

Co-localization of VE-cadherin and PA at AJs was quantified as described previously (72, 75). Briefly, for each image, the background signal was subtracted by drawing a region of interest around the cell periphery of individual cells. All areas outside the cell were cleared to best visualize the leading edges including cell periphery, and the fluorescence intensity within the entire cell was summed by MBF ImageJ bundle (Tony Collins, McMaster University and Wayne Rasband, NIH). PCC was used as a statistic for quantifying co-localization. PCC was defined by the following formula,

$$PCC = \frac{\sum_i (R_i - \bar{R}) \times (G_i - \bar{G})}{\sqrt{\sum_i (R_i - \bar{R})^2 \times \sum_i (G_i - \bar{G})^2}} \quad (\text{Eq. 1})$$

where R_i and G_i refer to the intensity values of the red and green channels, respectively, of pixel i , \bar{R} and \bar{G} refer to the mean intensities of the red and green channels, respectively, across the entire image. Values near 1 reflect the fluorescence intensities of two images that are perfectly and linearly related to one another. Values near zero reflect distribution of probes that are uncorrelated to one another.

Statistical analysis

Results are expressed as mean \pm S.D. of 3 to 5 independent experiments. Statistical significance was assessed by ANOVA followed by Newman Keuls post hoc test for the *in vivo* experiments, VE-cadherin intensity analysis, and ECIS permeability or the nonparametric Wold-Wolfowitz runs test for co-localization analysis. This statistical test was selected because it allows for the evaluation of two different kinds of statistical assumptions, binomial to determine whether co-localization is present or not, and Poisson to assess for the randomness of this co-localization. In all cases, statistical significance was defined at $p < 0.05$.

Data availability

All data presented and discussed are contained within the manuscript.

Acknowledgments—We thank Dr. Gilbert Di Paolo, Columbia University Medical Center, New York, for providing the PLD1 and PLD2 knockout mice.

Author contributions—P. F., R. R., M. S., L. H., D. L. E., Y. J., Y. K., S. M. V., A. B. M., R. D. M., G. D., N. K. T., and V. N. resources; P. F., R. R., Y. K., S. M. V., N. K. T., and V. N. investigation; P. F., N. K. T., and V. N. writing-original draft; P. F., R. R., S. M. V., A. B. M., R. D. M., G. D., N. K. T., and V. N. writing-review and editing; R. R. and V. N. validation; Y. J. methodology; N. K. T. and V. N. data curation; N. K. T. and V. N. supervision.

Funding and additional information—This work was supported by National Institutes of Health Grants HLBI P01 HL060678 (to V. N.) and AR075830 (to G. D.), and American Heart Association Grant 19TPA34910051. The content is solely the responsibility of the authors and does not necessarily represent the official views of the National Institutes of Health.

Conflict of interest—The authors declare that they have no conflicts of interest with the contents of this article.

Abbreviations—The abbreviations used are: ALI, acute lung injury; HLMVECs, human lung microvascular endothelial cells; EC, endothelial cell; PLD, phospholipase D; PA, phosphatidic acid; PTPN14, protein-tyrosine phosphatase N14; BAL, bronchoalveolar lavage; PAR-1-AP, protease-activated receptor-1-activating peptide; AJ, adhesion junctions; LPS, lipopolysaccharide; TIRF, total internal reflection fluorescence; RFP, red fluorescent protein; Thr, thrombin; IP, immunoprecipitation; PCC, Pearson's correlation coefficient; FBS, fetal bovine serum; EBM, endothelial basal medium; Pbt, phosphatidylbutanol; ECIS, electrical cell impedance; system; ANOVA, analysis of variance; TNF, tumor necrosis factor; VE, vascular endothelial; MLMVEC, mouse lung microvascular endothelial cell; TER, transendothelial electrical resistance; MOI, multiplicity of infection; H&E, hematoxylin and eosin.

References

1. Taddei, A., Giampietro, C., Conti, A., Orsenigo, F., Breviaro, F., Pirazzoli, V., Potente, M., Daly, C., Dimmeler, S., and Dejana, E. (2008) Endothelial adherens junctions control tight junctions by VE-cadherin-mediated up-regulation of claudin-5. *Nat. Cell Biol.* **10**, 923–934 [CrossRef Medline](#)
2. Dejana, E., Orsenigo, F., and Lampugnani, M. G. (2008) The role of adherens junctions and VE-cadherin in the control of vascular permeability. *J. Cell Sci.* **121**, 2115–2122 [CrossRef Medline](#)
3. Gavard, J. (2014) Endothelial permeability and VE-cadherin: a wacky comradeship. *Cell Adh. Migr.* **8**, 158–164 [CrossRef Medline](#)
4. Lee, W. L., and Slutsky, A. S. (2010) Sepsis and endothelial permeability. *N. Engl. J. Med.* **363**, 689–691 [CrossRef Medline](#)
5. Su, W., and Kowalczyk, A. P. (2017) The VE-cadherin cytoplasmic domain undergoes proteolytic processing during endocytosis. *Mol. Biol. Cell* **28**, 76–84 [CrossRef Medline](#)
6. Wu, Z., Wang, Z., Dai, F., Liu, H., Ren, W., Chang, J., and Li, B. (2016) Dephosphorylation of Y685-VE-cadherin involved in pulmonary microvascular endothelial barrier injury induced by angiotensin II. *Mediators Inflamm.* **2016**, 8696481 [Medline](#)
7. Wallez, Y., Cand, F., Cruzalegui, F., Wernstedt, C., Souchelnytskyi, S., Vilgrain, I., and Huber, P. (2007) Src kinase phosphorylates vascular en-

PLD2 regulation of barrier restoration via PTPN14 in endothelium

- dothelial-cadherin in response to vascular endothelial growth factor: identification of tyrosine 685 as the unique target site. *Oncogene* **26**, 1067–1077 [CrossRef Medline](#)
8. Wessel, F., Winderlich, M., Holm, M., Frye, M., Rivera-Galdos, R., Vockel, M., Linnepe, R., Ipe, U., Stadtmann, A., Zarbock, A., Nottebaum, A. F., and Vestweber, D. (2014) Leukocyte extravasation and vascular permeability are each controlled *in vivo* by different tyrosine residues of VE-cadherin. *Nat. Immunol.* **15**, 223–230 [CrossRef Medline](#)
 9. Gavard, J., Patel, V., and Gutkind, J. S. (2008) Angiopoietin-1 prevents VEGF-induced endothelial permeability by sequestering Src through mDia. *Dev. Cell* **14**, 25–36 [CrossRef Medline](#)
 10. Spring, K., Chabot, C., Langlois, S., Lapointe, L., Trinh, N. T., Caron, C., Hebda, J. K., Gavard, J., Elchebly, M., and Royal, I. (2012) Tyrosine phosphorylation of DEP-1/CD148 as a mechanism controlling Src kinase activation, endothelial cell permeability, invasion, and capillary formation. *Blood* **120**, 2745–2756 [CrossRef Medline](#)
 11. Chen, X. L., Nam, J. O., Jean, C., Lawson, C., Walsh, C. T., Goka, E., Lim, S. T., Tomar, A., Tancioni, I., Uryu, S., Guan, J. L., Acevedo, L. M., Weis, S. M., Cheresch, D. A., and Schlaepfer, D. D. (2012) VEGF-induced vascular permeability is mediated by FAK. *Dev. Cell* **22**, 146–157 [CrossRef Medline](#)
 12. Gavard, J., and Gutkind, J. S. (2006) VEGF controls endothelial-cell permeability by promoting the β -arrestin-dependent endocytosis of VE-cadherin. *Nat. Cell Biol.* **8**, 1223–1234 [CrossRef Medline](#)
 13. Gavard, J., and Gutkind, J. S. (2008) VE-cadherin and claudin-5: it takes two to tango. *Nat. Cell Biol.* **10**, 883–885 [CrossRef Medline](#)
 14. Nawroth, R., Poell, G., Ranft, A., Kloep, S., Samulowitz, U., Fachinger, G., Golding, M., Shima, D. T., Deutsch, U., and Vestweber, D. (2002) VE-PTP and VE-cadherin ectodomains interact to facilitate regulation of phosphorylation and cell contacts. *EMBO J.* **21**, 4885–4895 [CrossRef Medline](#)
 15. Nottebaum, A. F., Cagna, G., Winderlich, M., Gamp, A. C., Linnepe, R., Polaschegg, C., Filippova, K., Lyck, R., Engelhardt, B., Kamenyeva, O., Bixel, M. G., Butz, S., and Vestweber, D. (2008) VE-PTP maintains the endothelial barrier via plakoglobin and becomes dissociated from VE-cadherin by leukocytes and by VEGF. *J. Exp. Med.* **205**, 2929–2945 [CrossRef Medline](#)
 16. Broermann, A., Winderlich, M., Block, H., Frye, M., Rossaint, J., Zarbock, A., Cagna, G., Linnepe, R., Schulte, D., Nottebaum, A. F., and Vestweber, D. (2011) Dissociation of VE-PTP from VE-cadherin is required for leukocyte extravasation and for VEGF-induced vascular permeability *in vivo*. *J. Exp. Med.* **208**, 2393–2401 [CrossRef Medline](#)
 17. Giannotta, M., Trani, M., and Dejana, E. (2013) VE-cadherin and endothelial adherens junctions: active guardians of vascular integrity. *Dev. Cell* **26**, 441–454 [CrossRef Medline](#)
 18. Wadham, C., Gamble, J. R., Vadas, M. A., and Khew-Goodall, Y. (2003) The protein tyrosine phosphatase Pez is a major phosphatase of adherens junctions and dephosphorylates β -catenin. *Mol. Biol. Cell* **14**, 2520–2529 [CrossRef](#)
 19. Barr, A. J., Debreczeni, J. E., Eswaran, J., and Knapp, S. (2006) Crystal structure of human protein tyrosine phosphatase 14 (PTPN14) at 1.65-Å resolution. *Proteins* **63**, 1132–1136 [CrossRef Medline](#)
 20. Au, A. C., Hernandez, P. A., Lieber, E., Nadroo, A. M., Shen, Y. M., Kelley, K. A., Gelb, B. D., and Diaz, G. A. (2010) Protein tyrosine phosphatase PTPN14 is a regulator of lymphatic function and choanal development in humans. *Am. J. Hum. Genet.* **87**, 436–444 [CrossRef Medline](#)
 21. Benzinou, M., Clermont, F. F., Letteboer, T. G., Kim, J. H., Espejel, S., Harradine, K. A., Arbelaez, J., Luu, M. T., Roy, R., Quigley, D., Higgins, M. N., Zaid, M., Aouizerat, B. E., van Amstel, J. K., Giraud, S., *et al.* (2012) Mouse and human strategies identify PTPN14 as a modifier of angiogenesis and hereditary haemorrhagic telangiectasia. *Nat. Commun.* **3**, 616 [CrossRef Medline](#)
 22. Wilson, K. E., Li, Y. W., Yang, N., Shen, H., Orillion, A. R., and Zhang, J. (2014) PTPN14 forms a complex with Kibra and LATS1 proteins and negatively regulates the YAP oncogenic function. *J. Biol. Chem.* **289**, 23693–23700 [CrossRef Medline](#)
 23. Wang, W., Huang, J., Wang, X., Yuan, J., Li, X., Feng, L., Park, J. I., and Chen, J. J. (2012) PTPN14 is required for the density-dependent control of YAP1. *Gene Dev.* **26**, 1959–1971 [CrossRef Medline](#)
 24. Ramesh, M., Krishnan, N., Muthuswamy, S. K., and Tonks, N. K. (2015) A novel phosphatidic acid–protein-tyrosine phosphatase D2 axis is essential for ERBB2 signaling in mammary epithelial cells. *J. Biol. Chem.* **290**, 9646–9659 [CrossRef Medline](#)
 25. Zegarlińska, J., Piascik, M., Sikorski, A. F., and Czogalla, A. (2018) Phosphatidic acid: a simple phospholipid with multiple faces. *Acta Biochim. Pol.* **65**, 163–171 [CrossRef Medline](#)
 26. Ktistakis, N. T., Delon, C., Manifava, M., Wood, E., Ganley, I., and Sugars, J. M. (2003) Phospholipase D1 and potential targets of its hydrolysis product, phosphatidic acid. *Biochem. Soc. Trans.* **31**, 94–97 [CrossRef Medline](#)
 27. Nelson, R. K., and Frohman, M. A. (2015) Physiological and pathophysiological roles for phospholipase D. *J. Lipid Res.* **56**, 2229–2237 [CrossRef Medline](#)
 28. Abdunour, R. E., Howrylak, J. A., Tavares, A. H., Douda, D. N., Henkels, K. M., Miller, T. E., Fredenburgh, L. E., Baron, R. M., Gomez-Cambronero, J., and Levy, B. D. (2018) Phospholipase D isoforms differentially regulate leukocyte responses to acute lung injury. *J. Leukocyte Biol.* **103**, 919–932 [CrossRef Medline](#)
 29. Flores, I., Casaseca, T., Martinez-A., C., Kanoh, H., and Merida, I. (1996) Phosphatidic acid generation through interleukin 2 (IL-2)-induced α -diacylglycerol kinase activation is an essential step in IL-2-mediated lymphocyte proliferation. *J. Biol. Chem.* **271**, 10334–10340 [CrossRef Medline](#)
 30. Reeves, H. L., Thompson, M. G., Dack, C. L., Burt, A. D., and Day, C. P. (2000) The role of phosphatidic acid in platelet-derived growth factor-induced proliferation of rat hepatic stellate cells. *Hepatology* **31**, 95–100 [CrossRef Medline](#)
 31. Antonescu, C. N., Danuser, G., and Schmid, S. L. (2010) Phosphatidic acid plays a regulatory role in clathrin-mediated endocytosis. *Mol. Biol. Cell* **21**, 2944–2952 [CrossRef Medline](#)
 32. Jiang, Y., Sverdlov, M. S., Toth, P. T., Huang, L. S., Du, G., Liu, Y., Natarajan, V., and Minshall, R. D. (2016) Phosphatidic acid produced by RalA-activated PLD2 stimulates caveolae-mediated endocytosis and trafficking in endothelial cells. *J. Biol. Chem.* **291**, 20729–20738 [CrossRef Medline](#)
 33. Pleskot, R., Li, J., Zarský, V., Potocký, M., and Staiger, C. J. (2013) Regulation of cytoskeletal dynamics by phospholipase D and phosphatidic acid. *Trends Plant Sci.* **18**, 496–504 [CrossRef Medline](#)
 34. Roach, A. N., Wang, Z., Wu, P., Zhang, F., Chan, R. B., Yonekubo, Y., Di Paolo, G., Gorge, A. A., and Du, G. (2012) Phosphatidic acid regulation of PIPKI is critical for actin cytoskeletal reorganization. *J. Lipid Res.* **53**, 2598–2609 [CrossRef Medline](#)
 35. Rudge, S. A., and Wakelam, M. J. (2009) Inter-regulatory dynamics of phospholipase D and the actin cytoskeleton. *Biochim. Biophys. Acta* **1791**, 856–861 [CrossRef Medline](#)
 36. Agwu, D. E., McPhail, L. C., Sozzani, S., Bass, D. A., and McCall, C. E. (1991) Phosphatidic acid as a second messenger in human polymorphonuclear leukocytes: effects on activation of NADPH oxidase. *J. Clin. Invest.* **88**, 531–539 [CrossRef Medline](#)
 37. Jang, J. H., Lee, C. S., Hwang, D., and Ryu, S. H. (2012) Understanding of the roles of phospholipase D and phosphatidic acid through their binding partners. *Prog. Lipid Res.* **51**, 71–81 [CrossRef Medline](#)
 38. Coughlin, S. R. (2000) Thrombin signalling and protease-activated receptors. *Nature* **407**, 258–264 [CrossRef Medline](#)
 39. Vandenbroucke, E., Mehta, D., Minshall, R., and Malik, A. B. (2008) Regulation of endothelial junctional permeability. *Ann. N.Y. Acad. Sci.* **1123**, 134–145 [CrossRef Medline](#)
 40. Mukherjee, S., Tessema, M., and Wandinger-Ness, A. (2006) Vesicular trafficking of tyrosine kinase receptors and associated proteins in the regulation of signaling and vascular function. *Circ. Res.* **98**, 743–756 [CrossRef Medline](#)
 41. Garcia, J. G., Fenton, J. W., 2nd, and Natarajan, V. (1992) Thrombin stimulation of human endothelial cell phospholipase D activity: regulation by phospholipase C, protein kinase C, and cyclic adenosine 3'5'-monophosphate. *Blood* **79**, 2056–2067 [Medline](#)
 42. Garcia, J. G. (1992) Molecular mechanisms of thrombin-induced human and bovine endothelial cell activation. *J. Lab. Clin. Med.* **120**, 513–519 [Medline](#)
 43. Suryadevara, V., Huang, L., Kim, S.-J., Cheresch, P., Shaaya, M., Bandela, M., Fu, P., Feghali-Bostwick, C., Di Paolo, G., Kamp, D. W., and Natarajan,

- V. (2019) Role of phospholipase D in bleomycin-induced mitochondrial reactive oxygen species generation, mitochondrial DNA damage, and pulmonary fibrosis. *Am. J. Physiol. Lung Cell Mol. Physiol.* **317**, L175–L187 [CrossRef Medline](#)
44. Tian, X., Tian, Y., Gawlak, G., Sarich, N., Wu, T., and Birukova, A. A. (2014) Control of vascular permeability by atrial natriuretic peptide via a GEF-H1-dependent mechanism. *J. Biol. Chem.* **289**, 5168–5183 [CrossRef Medline](#)
45. Wang, L., Cummings, R., Usatyuk, P., Morris, A., Irani, K., and Natarajan, V. (2002) Role of phospholipase D-dependent-ERK activation in sphingophinc-1-phospholipid induced IL-8 secretions in human bronchial epithelial cells. *Biochem. J.* **367**, 751–760 [CrossRef Medline](#)
46. Lu, M., Tay, L. W., He, J., and Du, G. (2016) Monitoring phosphatidic acid signaling in breast cancer cells using genetically encoded biosensors. *Methods Mol. Biol.* **1406**, 225–237 [CrossRef Medline](#)
47. Zhang, F., Wang, Z., Lu, M., Yonekubo, Y., Liang, X., Zhang, Y., Wu, P., Zhou, Y., Grinstein, S., Hancock, J. F., and Du, G. (2014) Temporal production of the signaling lipid phosphatidic acid by phospholipase D2 determines the output of extracellular signal-regulated kinase signaling in cancer cells. *Mol. Cell Biol.* **34**, 84–95 [CrossRef Medline](#)
48. Harris, E. S., and Nelson, W. J. (2010) VE-cadherin: at the front, center, and sides of endothelial cell organization and function. *Curr. Opin. Cell Biol.* **22**, 651–658 [CrossRef Medline](#)
49. Ukropec, J. A., Hollinger, M. K., Salva, S. M., and Woolkalis, M. J. (2000) SHP2 association with VE-cadherin complexes in human endothelial cells is regulated by thrombin. *J. Biol. Chem.* **275**, 5983–5986 [CrossRef Medline](#)
50. Hu, G., Place, A. T., and Minshall, R. D. (2008) Regulation of endothelial permeability by Src kinase signaling: vascular leakage versus transcellular transport of drugs and macromolecules. *Chem. Biol. Interact.* **171**, 177–189 [CrossRef Medline](#)
51. Gong, H., Gao, X., Feng, S., Siddiqui, M. R., Garcia, A., Bonini, M. G., Komarova, Y., Vogel, S. M., Mehta, D., and Malik, A. B. (2014) Evidence of a common mechanism of disassembly of adherens junctions through Gα13 targeting VE-cadherin. *J. Exp. Med.* **211**, 579–591 [CrossRef Medline](#)
52. Adam, A. P. (2015) Regulation of endothelial adherens junctions by tyrosine phosphorylation. *Mediators Inflamm.* **2015**, 272858 [CrossRef](#)
53. Matthay, M. A., and Zemans, R. L. (2011) The acute respiratory distress syndrome: pathogenesis and treatment. *Annu. Rev. Pathol.* **6**, 147–163 [CrossRef Medline](#)
54. Matthay, M. A., Ware, L. B., and Zimmerman, G. A. (2012) The acute respiratory distress syndrome. *J. Clin. Invest.* **122**, 2731–2740 [CrossRef Medline](#)
55. Lim, H. K., Choi, Y. A., Park, W., Lee, T., Ryu, S. H., Kim, S. Y., Kim, J. R., Kim, J. H., and Baek, S. H. (2003) Phosphatidic acid regulates systemic inflammatory responses by modulating the Akt-mammalian target of rapamycin-p70 S6 kinase 1 pathway. *J. Biol. Chem.* **278**, 45117–45127 [CrossRef Medline](#)
56. Wang, Z., Cai, M., Tay, L. W. R., Zhang, F., Wu, P., Huynh, A., Cao, X., Di Paolo, G., Peng, J., Milewicz, D. M., and Du, G. (2019) Phosphatidic acid generated by PLD2 promotes the plasma membrane recruitment of IQGAP1 and neointima formation. *FASEB J.* **33**, 6713–6725 [CrossRef Medline](#)
57. Usatyuk, P. V., Kotha, S. R., Parinandi, N. L., and Natarajan, V. (2013) Phospholipase D signaling mediates reactive oxygen species-induced lung endothelial barrier dysfunction. *Pulm. Circ.* **3**, 108–115 [CrossRef Medline](#)
58. Zeiller, C., Mebarek, S., Jaafar, R., Pirolo, L., Lagarde, M., Prigent, A. F., and Némoz, G. (2009) Phospholipase D2 regulates endothelial permeability through cytoskeleton reorganization and occludin downregulation. *Biochim. Biophys. Acta* **1793**, 1236–1249 [CrossRef Medline](#)
59. Wu, M. H. (2005) Endothelial focal adhesions and barrier function. *J. Physiol.* **569**, 359–366 [CrossRef Medline](#)
60. Ebnet, K. (2008) Organization of multiprotein complexes at cell-cell junctions. *Histochem. Cell Biol.* **130**, 1–20 [CrossRef Medline](#)
61. Katso, R. M., Pardo, O. E., Palamidessi, A., Franz, C. M., Marinov, M., De Laurentiis, A., Downward, J., Scita, G., Ridley, A. J., Waterfield, M. D., and Arcaro, A. (2006) Phosphoinositide 3-kinase C2β regulates cytoskeletal organization and cell migration via Rac-dependent mechanisms. *Mol. Biol. Cell* **17**, 3729–3744 [CrossRef Medline](#)
62. Yamada, S., and Nelson, W. J. (2007) Localized zones of Rho and Rac activities drive initiation and expansion of epithelial cell-cell adhesion. *J. Cell Biol.* **178**, 517–527 [CrossRef Medline](#)
63. Xiao, K., Garner, J., Buckley, K. M., Vincent, P. A., Chiasson, C. M., Dejana, E., Faundez, V., and Kowalczyk, A. P. (2005) p120-Catenin regulates clathrin-dependent endocytosis of VE-cadherin. *Mol. Biol. Cell* **16**, 5141–5151 [CrossRef Medline](#)
64. Soni, D., Regmi, S. C., Wang, D. M., DebRoy, A., Zhao, Y. Y., Vogel, S. M., Malik, A. B., and Tiruppathi, C. (2017) Pyk2 phosphorylation of VE-PTP downstream of STIM1-induced Ca²⁺ entry regulates disassembly of adherens junctions. *Am. J. Physiol. Lung Cell Mol. Physiol.* **312**, L1003–L1017 [CrossRef Medline](#)
65. Sui, X. F., Kiser, T. D., Hyun, S. W., Angelini, D. J., Del Vecchio, R. L., Young, B. A., Hasday, J. D., Romer, L. H., Passaniti, A., Tonks, N. K., and Goldblum, S. E. (2005) Receptor protein tyrosine phosphatase micro regulates the paracellular pathway in human lung microvascular endothelia. *Am. J. Pathol.* **166**, 1247–1258 [CrossRef Medline](#)
66. Juettner, V. V., Kruse, K., Dan, A., Vu, V. H., Khan, Y., Le, J., Leckband, D., Komarova, Y., and Malik, A. B. (2019) VE-PTP stabilizes VE-cadherin junctions and the endothelial barrier via a phosphatase-independent mechanism. *J. Cell Biol.* **218**, 1725–1742 [CrossRef Medline](#)
67. Kowalczyk, A. P., and Nanes, B. A. (2012) Adherens junction turnover: regulating adhesion through cadherin endocytosis, degradation, and recycling. *Subcell. Biochem.* **60**, 197–222 [CrossRef Medline](#)
68. Wang, Z., Zhang, F., He, J., Wu, P., Tay, L. W. R., Cai, M., Nian, W., Weng, Y., Qin, L., Chang, J. T., McIntire, L. B., Di Paolo, G., Xu, J., Peng, J., and Du, G. (2017) Binding of PLD2-generated phosphatidic acid to KIF5B promotes MT1-MMP surface trafficking and lung metastasis of mouse breast cancer cells. *Dev. Cell* **43**, 186–197.e7 [CrossRef Medline](#)
69. Bolomini-Vittori, M., Mennens, S. F. B., Joosten, B., Fransen, J., Du, G., van den Dries, K., and Cambi, A. (2019) PLD-dependent phosphatidic acid microdomains are signaling platforms for podosome formation. *Sci. Rep.* **9**, 3556 [CrossRef Medline](#)
70. Frye, M., Dierkes, M., Küppers, V., Vockel, M., Tomm, J., Zeuschner, D., Rossaint, J., Zarbock, A., Koh, G. Y., Peters, K., Nottebaum, A. F., and Vestweber, D. (2015) Interfering with VE-PTP stabilizes endothelial junctions in vivo via Tie-2 in the absence of VE-cadherin. *J. Exp. Med.* **212**, 2267–2287 [CrossRef Medline](#)
71. Han, X., Sun, T., Hong, J., Wei, R., Dong, Y., Huang, D., Chen, J., Ren, X., Zhou, H., Tian, W., and Jia, Y. (2019) Nonreceptor tyrosine phosphatase 14 promotes proliferation and migration through regulating phosphorylation of YAP of Hippo signaling pathway in gastric cancer cells. *J. Cell Biochem.* **120**, 17723–17730 [CrossRef Medline](#)
72. Usatyuk, P. V., Fu, P., Mohan, V., Epshtein, Y., Jacobson, J. R., Gomez-Cambronero, J., Wary, K. K., Bindokas, V., Dudek, S. M., Salgia, R., Garcia, J. G., and Natarajan, V. (2014) Role of c-Met/phosphatidylinositol 3-kinase (PI3k)/Akt signaling in hepatocyte growth factor (HGF)-mediated lamellipodia formation, reactive oxygen species (ROS) generation, and motility of lung endothelial cells. *J. Biol. Chem.* **289**, 13476–13491 [CrossRef Medline](#)
73. Tiruppathi, C., Freichel, M., Vogel, S. M., Paria, B. C., Mehta, D., Flockerzi, V., and Malik, A. B. (2002) Impairment of store-operated Ca²⁺ entry in TRPC4^{-/-} mice interferes with increase in lung microvascular permeability. *Circ. Res.* **91**, 70–76 [CrossRef Medline](#)
74. Usatyuk, P. V., Burns, M., Mohan, V., Pendyala, S., He, D., Ebenezer, D. L., Harijith, A., Fu, P., Huang, L. S., Bear, J. E., Garcia, J. G., and Natarajan, V. (2013) Coronin 1B regulates S1P-induced human lung endothelial cell chemotaxis: role of PLD2, protein kinase C and Rac1 signal transduction. *PLoS ONE* **8**, e63007 [CrossRef Medline](#)
75. Fu, P., Ebenezer, D. L., Berdyshev, E. V., Bronova, I. A., Shaaya, M., Harijith, A., and Natarajan, V. (2016) Role of sphingosine kinase 1 and S1P transporter Spns2 in HGF mediated lamellipodia formation in lung endothelium. *J. Biol. Chem.* **291**, 27187–27203 [CrossRef Medline](#)